Frequency Synchronisation of a Two-Level Quantum System

Erlend Andreas Longva

Thesis submitted for the degree of
Master in Materials, Nanophysics and Quantum Technology
60 credits

Department of Physics
The Faculty of Mathematics and Natural Sciences

UNIVERSITY OF OSLO

Spring 2022

Frequency Synchronisation of a Two-Level Quantum System

Erlend Andreas Longva

Frequency Synchronisation of a Two-Level Quantum System

http://www.duo.uio.no/

Printed: Reprosentralen, University of Oslo

Abstract

Quantum synchronisation has seen rapid development over the last few years. It was argued that a two-level system lacks a valid limit cycle, and so could not be synchronised.[1] However, with a different definition of synchronisation, the issue was resolved and it was shown that a two-level system can phase lock to an external signal.[2] Recently, an experiment has confirmed that a two-level systems can synchronise to an external signal.[3] Phase locking has been found using the Lindblad master equation, however, this method is unable to study the average frequency of the system. We attempt to resolve this by using quantum trajectory theory, giving us pure state unravelings of the Lindblad equation that we can calculate the frequency of. We demonstrate that two interactions between system and environment can replicate the Lindblad equation. The interactions are then used in a numerical simulation to measure the average frequency of a two-level system. We are able to show that a two-level system can frequency lock to an external signal, with behaviour similar to classical synchronisation with noise.

Contents

Acknowledgements

Studying physics have not only given me a better understanding of nature, but also made me greatly appreciate science. It is a very human endeavour, and all scientists are in a way deeply connected to each other. Like Newton, I too believe we see further because of the accomplishments of the many that came before us. But it is not only those that came before us that are lifting us up to see further, it is also those standing besides us in the present. As humans, and scientists, we must always remember that life and science are both collective efforts. I will not attempt to challenge John Cleese's famous world record, but there are a few people I would like to thank.

First and foremost, I wish to deeply thank my supervisor, professor Joakim Bergli for providing such an interesting topic to study. His supervision and guidance has been excellent, and I will greatly miss working with him. His quick correspondence and accessibility has meant a lot to me during this challenging, and often stressful period. Additionally, I would like to thank the University of Oslo for taking good care of me during my time as a student.

Coming from a family of educators has made me appreciate the significant impact great teachers can have on our lives. I am therefore very thankful of all the teachers that have helped me along the way. I especially thank Inga Hanne Dokka for igniting my interest in physics, and for her outstanding teaching at Kongsberg videregående skole.

I would like to thank all friends for supporting me and cheering me on during the course of my studies. Brage Medhus, Bendik Selvaag-Hagen, Alexander Wennevold Silva are amazing friends and I am very thankful for all their motivation and support. I also thank my fellow physics students Aron Jansson Nordberg and Frida Larsen for their friendship and support during my time at the University. I am deeply thankful for the help, support and friendship of Nils Johannes Mikkelsen, without you I would never be writing this right now.

I am very grateful for the support of my family. My parents have helped me in so many ways during my time as a student and I am very thankful for their love and motivation. I also wish to thank my sister for all her help and kindness, and for always being someone I can look up to.

Introduction

Synchronisation is a strikingly universal concept, observed in a diverse range of physical systems. It can be observed in biological systems, such as humans, ranging from heartbeat to circadian rhythm. It can also be observed in larger systems, such as an applauding crowd and swarms of fireflies flashing in synchronicity. The phenomenon is widely used in electronics to synchronise clocks, and the frequency of generators. And, as we will see, it even applies to the smallest possible system, a quantum two-level system.

It was first discovered by Christiaan Huygens, a famous Dutch mathematician, physicist and astronomer. While being sick he was confined to his room where he was watching two clocks suspended from a wooden beam. He observed that the clocks synchronised and deduced that this was caused by some imperceptible motion of the beam. In other words, by letting two autonomous oscillators interact weakly their frequency and phase will synchronise, referred to as frequency and phase locking.

It has previously been shown that the synchronisation behavior of a quantum mechanical system can be modelled as a classical system with noise.[2] This article demonstrates that a quantum two-level system can achieve phase synchronisation with an external signal, but not full phase locking because the phase is perturbed by the noise.

In this thesis we develop a model based on quantum trajectory theory[4] which enables us to directly measure the frequency of several pure states. This is not possible using the standard description of such a system, the Lindblad master equation. The solution of the master equation is the density matrix of the system, which is a mixed state, and hence a statistical mix of many possible pure states. Trajectory theory gives us an *unraveling* of the master equation, giving us the possible trajectories of the many pure states that, on average, reproduce the statistical mix given by the master equation.

Our goal is therefore to identify one or more possible unravelings for a two-level system capable of synchronisation, and then use this in a numerical simulation to find the average frequency of the system when synchronising it to an external signal. We demonstrate that quantum trajectory theory can be used to create a model of a two-level system with a limit cycle. This is achieved by identifying two interactions, corresponding to absorption and emission, that replicate the Lindblad master equation used in [2]. Furthermore, we are able to numerically simulate the two-level system synchronising to an external signal, finding frequency synchronisation with behaviour similar to that of classical synchronisation with noise.

Chapter 1

Background material

The background material we have used in the development of our model consists of theory from classical synchronisation, some previous results from quantum synchronisation, and quantum trajectory theory. We first provide some basic insight into classical synchronisation, where we explain what is meant by synchronisation and the characteristics of systems exhibiting this behaviour. Importantly, this section ends with a short description of classical synchronisation with noise.

We then discuss previous results and recent developments concerning quantum synchronisation, before going through the main motivation behind our investigation, that is, the article[2] by Álvaro Parra-López and Joakim Bergli. We show how the Lindblad master equation can be solved analytically for a two-level system, and explain why the system can be considered to have a valid limit cycle. Then we show how the system can phase lock with a weak external signal, and explain how the strength of the synchronisation can be visualised.

The last part of the chapter is dedicated to quantum trajectory theory. We first explain what the trajectories are and the scheme used to find them. Then we look at the form of the interactions we consider, and two kinds of weak measurements we can obtain by using the theory. Lastly, we show how to recover the Lindblad master equation from trajectory theory. This part is especially important to follow the derivation of interactions done in 2.1.1.

1.1 Synchronisation

The phenomenon of synchronisation is found many places in nature. It has been extensively studied, and used in several technologies. It was first described by Christiaan Huygens (1629-1695) in 1673. The phenomenon can be observed in physical systems ranging from our own circadian rhythm, two pendulum clocks hanging on a wall, the sinoatrial nodes responsible for the beating of our heart, to nanomechanical oscillators.[5] We first go through the classical description of synchronisation, where we explain what is meant by a self-sustained oscillator and the limit cycle, and then briefly explain classical synchronisation with noise. The more recent development in quantum synchronisation is then discussed before we show how a quantum

two-level system can phase lock its dynamics to a weak external signal.[2]

1.1.1 Classical Synchronisation

Here we introduce the concept of synchronisation in the classical sense, explaining the necessary conditions, properties and main features. All the presented material is based on the excellent book [6] by Pikovsky, Rosenblum and Kurths. Loosely speaking, the phenomenon is self-explanatory in that it is the synchronisation of two or more oscillating systems. A simple form of synchronisation can be visualised by placing two metronomes on top of a skateboard. Each metronome has a frequency f and a difference, or detuning, $\Delta f = f_1 - f_2$ of their respective frequencies. With each oscillation, the metronomes will give the skateboard a weak push, thereby slightly displacing it. One metronome pushing the skateboard also pushes the second metronome, hence, slightly perturbing its oscillations. If we leave this system like this for a while the metronomes will soon start oscillating with the same frequency, and we observe synchronisation. Placing the metronomes back on a steady surface results in their frequencies returning to the original asynchronous state.

The previous example illustrates most of the necessary conditions for synchronisation to occur. A metronome is a self-sustained oscillator because of its internal energy source. It is also dissipative, losing some energy to its environment due to air resistance. Both of these features are necessary for a system to synchronise. The second important condition, is that the two systems are coupled by a *weak* interaction. If we, on the other hand, connected the metronomes with a metal bar, their oscillations would naturally be synchronous. Clearly, this "interaction" does not provide us with synchronisation. The coupling between the oscillators should, in a sense, be weak compared to the internal driving force. There is no exact definition of when an interaction is too strong. However, the interactions can be extremely weak and still make the metronomes synchronise, which is what makes the phenomenon interesting to study. Instead of having two or more oscillators synchronise by being coupled with each other, we can have one oscillator and synchronise this to a weak external signal. This can be thought of as being the second metronome in our example, but in this case it would not itself be influenced by the weak coupling. Instead, it would retain its original frequency, which the first metronome would synchronise to. This kind of synchronisation is what we use in our model.

A useful way to characterise self-sustained oscillators is by representing them in the phase space. The variables needed to unambiguously specify the system state defines a closed curve in phase space. This is the system's *limit cycle*. Importantly, self-sustained oscillators will return to their limit cycle after small perturbations. This can be illustrated by a quasilinear oscillator with a limit cycle given by the sine wave $x(t) = A\sin(\omega_0 t + \phi_0)$, where ω_0 is the angular frequency, A is the amplitude and $\phi(t) = \omega_0 t + \phi_0$ is the phase, with ϕ_0 being the initial phase. Using A and $\phi(t)$ as the phase space variables, we can represent the oscillators limit cycle in the phase space. For convenience we do this in a reference frame rotating counter-clockwise with

angular frequency ω_0, so that the unperturbed oscillator has a stationary phase point. This is shown in figure 1.1, and illustrates the behaviour of a self-sustained oscillator after a perturbation. Looking at (b) in the figure, we observe that perturbations on the system can permanently change the phase, and while the amplitude remains stable the phase is free. The phase can be freely perturbed by an outside force. Hence, it is capable of synchronisation.

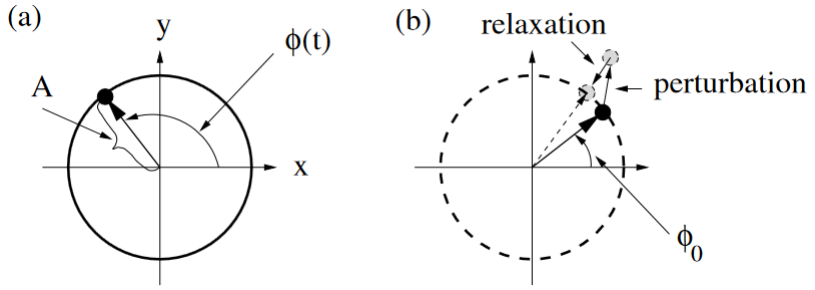

Figure 1.1: (a) The unperturbed self-sustained oscillator at a stationary phase point on the limit cycle, using the amplitude A and the phase $\phi(t)$ as the phase space variables. (b) The oscillator after a small perturbation. Observe that after relaxation the amplitude is preserved while the phase is perturbed. This figure is copied from [6].

Let us build on this by introducing a weak external force on the system, of the form $F_e(t) = \epsilon\cos(\omega t + \phi_e')$, where ϵ is the strength, ω the angular frequency and $\phi_e = \omega t + \phi_e'$ the phase. The detuning is then $\Delta = \omega - \omega_0$. We now change the reference frame to that of the external force, such that it is rotating counter-clockwise with frequency ω. This is useful because we are interested in the effect of the detuning. When $\omega_0 = \omega$ the detuning is 0 and the phase space angle $\phi - \phi_e$ is stationary. The limit cycle of this system is shown in figure 1.2 where the force is assumed to have no amplitude, hence, strength $\epsilon = 0$.

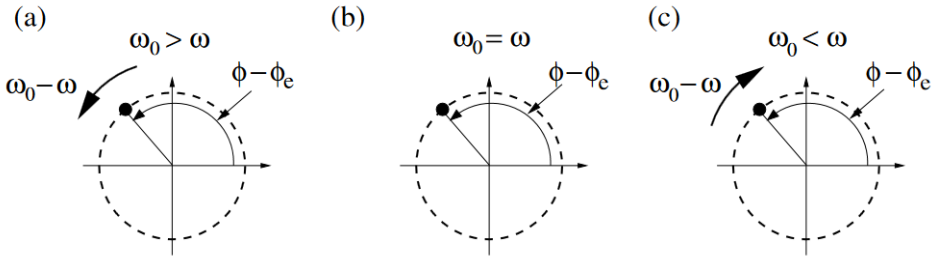

Figure 1.2: The limit cycle of a quasilinear oscillator subjected to an external force, the reference frame rotating counter-clockwise with the frequency ω of the force. (a) The angle variable $\phi - \phi_e$ increases, (b) is stationary, (c) decreases. This figure is copied from [6].

When the force is turned on it will have the effect of perturbing the angle by a constant vector of length ϵ and some angle ϕ^0. Because of

this constant angle, which loosely corresponds to the force's initial angle ϕ'_e, the effect on the systems phase space angle will change along the limit cycle. There are then two points on the limit cycle where the perturbation acts perpendicular, one radially outwards, the other radially inwards. The different perturbations can be seen in figure 1.3. The perturbation in point 1 is the stable equilibrium, while point 2 is unstable. This is easily understood as the force pushing the phase space coordinate of the oscillator away from point 2 and towards point 1.

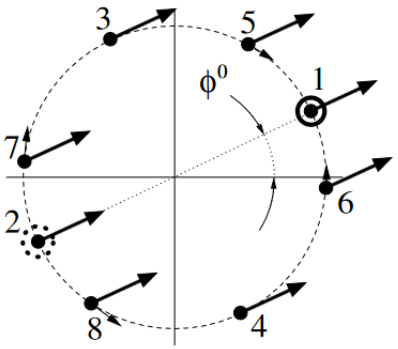

Figure 1.3: The perturbations caused by an external force acting on a quasilinear oscillator. We observe that the perturbations all move the phase space coordinate along the limit cycle towards the stable equilibrium (1). This figure is copied from [6].

We now move on to phase and frequency locking. First we introduce a new term, the observed frequency Ω. Consider the initial example of the two metronomes, each have some preset (natural) frequency f_1 and f_2. When we introduce some weak coupling between the metronomes, their frequencies will start to change, instead giving us some observed frequencies Ω_1 and Ω_2. The same is true for a quasilinear oscillator subjected to the external force. If we let the detuning be sufficiently small, there will be a some angle in phase space where the force balances the rotation and stops the motion of the phase point. This results in a constant phase shift, and so the observed frequency is equal to the frequency of the external force $\Omega = \omega$. When this occurs we say that the oscillator is phase locked with the external force, and unsurprisingly, in this case they are also frequency locked.

As we just discussed, locking occurs if the detuning is sufficiently small. This can be visualised by comparing the observed frequency Ω with the detuning Δ. In figure 1.4 a comparison is shown, and we observe that there is a region in which the oscillator remains perfectly frequency locked with the external force, but outside this region it increasingly tends towards its natural frequency ω_0. A third dimension to this is the strength of the force ϵ, which when increased expands the synchronisation region. This is shown in (b) and (c), the latter is known as the Arnold tongue of the system.

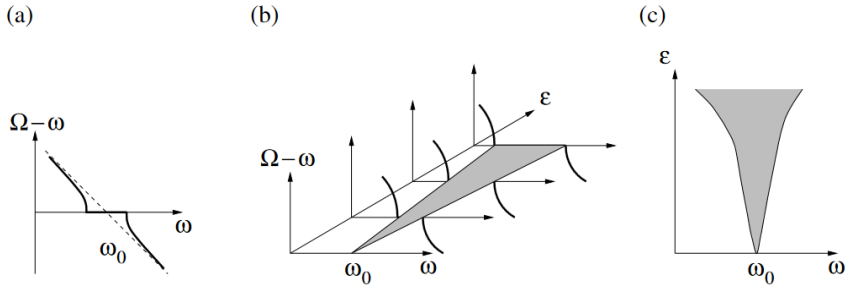

Figure 1.4: (a) Difference between the observed frequency of the oscillator Ω and the external force ω as a function of ω, clearly showing a region of frequency locking. (b) The synchronisation region (in gray) shown for increasing external force strength ϵ. (c) Representation of the synchronisation region (in gray) known as the Arnold tongue. This figure is copied from [6].

For our purpose of studying the frequency synchronisation of a two-level quantum system with an external signal (corresponding to the external force above), we want to find a curve similar to that shown in 1.4 (a). But the quantum mechanical description is stochastic, hence, it introduces randomness and therefore noise to the frequency of the system. This causes the phase point to diffuse around the deterministic stable equilibrium point on the limit cycle. Therefore, we look at the classical description of synchronisation with noise. The classical behaviour of synchronisation with noise is shown in figure 1.5, where (a) shows the synchronisation region for bounded and (b) for unbounded noise. If the noise of the system is bounded, there is a region where the system will remain fully frequency locked, but because of the noise, it is smaller. On the other hand, if the noise is unbounded, there is a certain probability, increased by the detuning, that the phase diffuses far enough away from the phase space equilibrium point, and so makes a rotation on the limit cycle. This is called a phase slip, and so, when the noise is unbounded, the system is only fully synchronised when the detuning is zero.

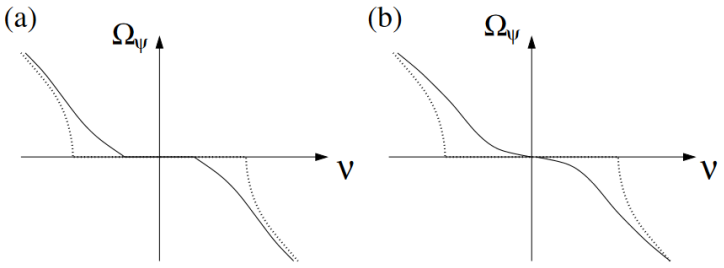

Figure 1.5: In the reference frame rotating with the external signal, Ω_ψ is the measured frequency and ν the detuning, (a) the system with bounded noise and (b) with unbounded noise. The dotted line is the corresponding behaviour without noise. This figure is copied from [6].

1.1.2 Quantum synchronisation

Early developments in the field of quantum synchronisation was for the most part theoretical investigations of the quantised driven van der Pol oscillator[7][8][9], along with proposals for realising this experimentally using nanomechanical oscillators.[5][10]

Some alternatives, with no classical analog, were suggested as candidates for studying quantum synchronisation, where the contributions by Roulet and Bruder have been important.[1] They proposed a spin-1 system subjected to an external signal as a candidate system, and found the existence of a limit cycle and synchronisation region theoretically. This has later been confirmed by experiments.[11] It was suggested in [1] that a three-level system was the smallest possible system able to synchronise, because it was argued that qubits could not have a limit cycle. The argument was that the probabilistic mixture of states, which the density matrix of the system is made of, would all be some eigenstates lying on the rotation axis. And so a phase variable for these states can not be found. However, this argument is open to interpretation, and in [2] Parra-López and Bergli is able to identify an interpretation allowing a limit cycle for the system.

New experimental results suggest that synchronisation of a single qubit to an external signal[3] is indeed possible. Furthermore, a very recent article studies synchronisation, theoretically, in a hybrid optoelectromechanical system, where a superconducting qubit is synchronised to an external optical field via a mechanical resonator.[12] The article shows phase synchronisation between a qubit and optical field via a resonator, using quantum trajectory theory to simulate the system. Another recent article, studying two superconducting qubits interacting with a resonator, theoretically demonstrates an effective synchronisation.[13]

The following theory is based on the previous work done by Parra-López and Bergli.[2] We focus on covering the important physics describing the system, and briefly cover the results obtained. The model we develop using quantum trajectory theory differs quite a lot from what is covered here, therefore, this section mostly serves as a concise introduction. The stationary solution of the Lindblad equation can be thought of as a mix of pure states lying on a circle on the surface of the Bloch sphere, in the plane normal to the z-axis. By interpreting the quantum system as a classical system with noise, these pure states then give us a valid limit cycle. Furthermore, the system can then be phase locked to a weak external signal. The system and Lindblad master equation used in the article forms the basis for the model we develop later on, using quantum trajectory theory.

We must first define a dissipative two-level system having some natural frequency ω_0, so that a stable limit cycle can be found. Hence, we consider a system described by the Hamiltonian

$$H_0 = \frac{\hbar}{2}\omega_0\sigma_z.$$

Additionally, the system can be described by a density matrix on the general

form

$$\rho' = \frac{1}{2}\big(\mathbb{1} + \mathbf{m}' \cdot \boldsymbol{\sigma}\big),$$

where $\mathbf{m}'$ is the Bloch vector, and $\boldsymbol{\sigma}$ a vector containing the Pauli matrices. We may transform to a frame rotating with ω_0 Using the transformation $T_{\omega_0} = \exp(i\omega_0\sigma_z t/2)$, such that, $\rho = T_{\omega_0}\rho' T_{\omega_0}^\dagger$, the Bloch vector in the new frame is denoted as $\mathbf{m}$. The Lindblad equation, in a reference frame rotating with ω_0, is

$$\begin{aligned}\frac{\mathrm{d}\rho}{\mathrm{d}t} = &\frac{\Gamma_+}{2}\left[\sigma_+\rho\sigma_+^\dagger - \frac{1}{2}\Big(\sigma_+^\dagger\sigma_+\rho + \rho\sigma_+^\dagger\sigma_+\Big)\right] \\ &+ \frac{\Gamma_-}{2}\left[\sigma_-\rho\sigma_-^\dagger - \frac{1}{2}\Big(\sigma_-^\dagger\sigma_-\rho + \rho\sigma_-^\dagger\sigma_-\Big)\right].\end{aligned}$$

In this equation, Γ_+ and Γ_- are the absorption and emission rates, respectively. These corresponds to the gain and damping of the dissipative system. We also use the ladder operators $\sigma_\pm = (\sigma_x \pm i\sigma_y)/2$. Then, using $\dot{\mathbf{m}} = 0$, the stationary solution is found to be

$$m_x = 0; \quad m_y = 0; \quad m_z = \frac{\Gamma_+ - \Gamma_-}{\Gamma_+ + \Gamma_-}.$$

The stationary solutions can then be represented on the surface of the Bloch sphere as a mixture of pure states, in a plane normal to the z-axis, as shown in figure 1.6. Importantly, the system is not in a superposition of these states, but certainly in one of them at any time. Seeing as these states will precess around the z-axis in the non-rotating reference frame, we get a limit cycle.

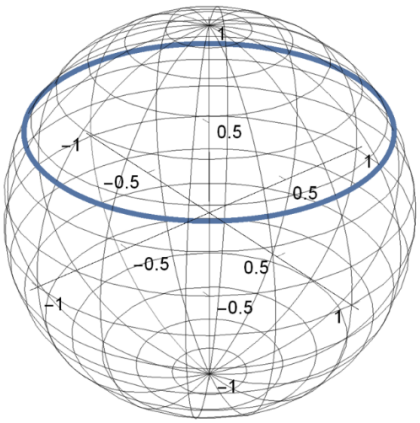

Figure 1.6: We may realise the stationary solution as a probabilistic mixture of pure states in the plane normal to the z-axis, lying on the blue circle. Each state moves along the same circle, with a periodic motion, and so gives rise to a limit cycle. In this figure $\Gamma_+/\Gamma_- = 3$ was used as the transition rate ratio. This figure is copied from [2].

The system is then synchronised to a weak signal, using a classical drive in the rotating wave approximation. This is described by the Hamiltonian

$$H_{\text{signal}} = i\hbar\frac{\epsilon}{4}\big(e^{i\omega t}\sigma_- - e^{-i\omega t}\sigma_+\big),$$

where ω is the frequency and ϵ the signal strength parameter. This time, we transform to a frame instead rotating with the signal, and so we use the transformation

$$T_\omega = e^{i\frac{\omega}{2}\sigma_z t},$$

resulting in the Lindblad equation

$$\begin{aligned}\frac{\mathrm{d}\rho}{\mathrm{d}t} = &-\frac{i}{2}\left[\Delta\sigma_z + \epsilon\sigma_y, \rho\right] + \frac{\Gamma_+}{2}\left[\sigma_+\rho\sigma_+^\dagger - \frac{1}{2}\left(\sigma_+^\dagger\sigma_+\rho + \rho\sigma_+^\dagger\sigma_+\right)\right] \\ &+ \frac{\Gamma_-}{2}\left[\sigma_-\rho\sigma_-^\dagger - \frac{1}{2}\left(\sigma_-^\dagger\sigma_-\rho + \rho\sigma_-^\dagger\sigma_-\right)\right].\end{aligned}$$

where Δ is the detuning $\omega_0 - \omega$. From this, we again find the stationary solution

$$m_x = \frac{4\epsilon(\Gamma_+ - \Gamma_-)}{(\Gamma_- + \Gamma_+)^2 + 8(\epsilon^2 + 2\Delta^2)}, \tag{1.1}$$

$$m_x = \frac{16\epsilon\Delta(\Gamma_+ - \Gamma_-)}{(\Gamma_- + \Gamma_+)\Big[(\Gamma_- + \Gamma_+)^2 + 8(\epsilon^2 + 2\Delta^2)\Big]}, \tag{1.2}$$

$$m_x = \frac{(\Gamma_- - \Gamma_+)\Big[(\Gamma_- + \Gamma_+)^2 + 16\Delta^2\Big]}{(\Gamma_- + \Gamma_+)\Big[(\Gamma_- + \Gamma_+)^2 + 8(\epsilon^2 + 2\Delta^2)\Big]}. \tag{1.3}$$

We can then transform back to obtain the state operator in the non-rotating reference frame, using the relation $\rho' = T_\omega^\dagger \rho T_\omega$. Giving us the Bloch vector components

$$\begin{aligned}m_x' &= m_x\cos(\omega t) - m_y\sin(\omega t), \\ m_y' &= m_x\sin(\omega t) + m_y\cos(\omega t), \\ m_z' &= m_z.\end{aligned}$$

We observe that m_x' and m_y' evolves in time with the frequency of the signal, hence, phase locking the system to the external force.

The phase space of a two-level system can be represented using the Husimi Q quasi-probability distribution, defined by

$$Q(\theta,\phi) = \frac{1}{2\pi}\left\langle\rho|\theta,\phi|\rho\right\rangle.$$

Here, θ and ϕ are the polar coordinates of the Bloch sphere. The states $|\theta,\phi\rangle$ are the eigenstates of the spin operator $\sigma_{\mathbf{n}} = \mathbf{n}\cdot\boldsymbol{\sigma}$ along the axis of the unit vector $\mathbf{n}$ in the direction given by the polar coordinates. Representing the stationary solution (1.1) in this way, we get the Q-function in terms of the Bloch vector components as

$$Q(\theta,\phi) = \frac{1}{4\pi}[1 + m_x\cos\phi\sin\theta + m_y\sin\phi\sin\theta + m_z\cos\theta].$$

In our case, the value of $Q(\theta, \phi)$ is a measure of how much every pure state on the Bloch sphere contributes to the density matrix, of the stationary solution. Additionally, one can measure the strength of synchronisation using the *synchronisation measure*, which is on the form

$$S(\phi) = \int_0^\pi d\theta \sin\theta Q(\theta, \phi) - \frac{1}{2\pi}.$$

Solving the integral for the stationary solution, we get

$$S(\phi) = \frac{1}{8}(m_x \cos\phi + m_y \sin\phi).$$

The Arnold tongue of the system can be found by varying the signal strength ϵ and the detuning Δ, and for each point (ϵ, Δ) finding the maximum value of the synchronisation measure $S(\phi)$. This corresponds to what was shown for classic synchronisation in figure 1.4 (c), but the behaviour is in this case diffusive.

1.2 Quantum trajectory theory

Here we cover the essential parts of quantum trajectory theory used to develop the numerical model later in the thesis. The theory was developed by Howard Carmichael[14] in the early 1990s, initially for the field of quantum optics. All material covered follows closely to the article by Todd A. Brun [4]. The theory can be used to describe the time evolution of open quantum systems by monitoring the environment they interact with. Open quantum systems, in this sense, are systems interacting with an environment. For all of the theory we discuss here, we restrict ourselves to studying two-level systems, or quantum bits (qubits). The use of this theory has largely belonged to the field of quantum optics, but has also garnered interest in the fields of quantum foundations and measurement theory.

In the following sections we begin with a brief overview of theory, explaining how monitoring successive interactions between system and environment enables us to find trajectories. We briefly discuss a possible physical realisation of such a process, before clarifying some of the simplifications we use. Next we discuss interactions and measurements, where we specify the form of the weak interaction and the behaviours that can result from weak measurements. Finally, the relation between trajectories and master equation is shown, providing the theoretical framework linking interactions to Lindblad operators.

1.2.1 Introduction

Our reason for using quantum trajectory theory, QTT, is to find the average frequency of a two-level system. This is not obtainable from the Lindblad master equation because its solution is a statistical mix, represented by a density matrix, of an ensemble of pure states. QTT allows us to simulate such an ensemble consisting of several trajectories, that on average, approximates the master equation solution. This is what is meant by unraveling the master

equation. We can then find the frequency of each single trajectory, and by taking the average for several trajectories, we find the average frequency of the two-level system.

Trajectories are found by simulating an open system which is successively interacting with a monitored environment. A simplified version of this process is shown in figure 1.7. In the figure we see how, for each time step δt, an environment qubit $|E\rangle$ interacts with the system $|\psi\rangle$ and is subsequently measured. After the interaction, $|\psi\rangle$ and $|E\rangle$ are entangled. We would therefore expect that measuring $|E\rangle$ disturbs the system, and in doing so the time evolution. In QTT this problem is solved by making the interaction U weak, close to a unitary operator, and so only a small amount of information about the system is obtained in each measurement. Because of this, the system is allowed to evolve, and with the information obtained by measuring $|E\rangle$, we can construct its trajectory.

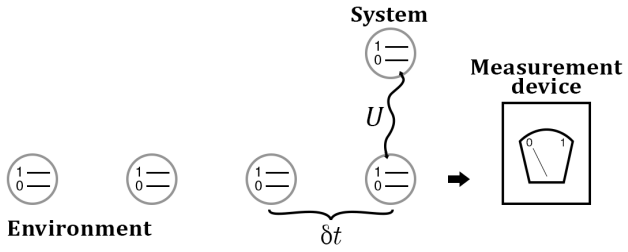

Figure 1.7: Schematic representation of the quantum trajectories method. At each time step δt, an environment qubit interacts with the system state and is subsequently measured. New environment qubits successively interacts, and are measured, in the same way.

An approximate physical realisation of this is explained in [4], where an electromagnetic mode is trapped inside a cavity together with a single photon. We can assume the cavity to be completely reflective, and so the system has no energy loss, and the photon never escapes. We then allow some atoms to successively pass through the cavity, measuring them afterwards. These atoms can be realised as Rydberg atoms being in a superposition of two neighbouring electronic states. The electronic state of these atoms are then measured upon leaving the cavity. The Rydberg atoms serve both as environment and measurement probe of the system, making it a good representation of the process that we study.

The evolution of the two-level system that we consider uses some important simplifications. The system qubit is in a state $|\psi\rangle$ in Hilbert space $\mathcal{H}_S = \mathcal{H}_2$ with Hamiltonian H_S, and the environment is similarly in state $|E\rangle \in \mathcal{H}_E = \mathcal{H}_2$ with Hamiltonian H_E. And so their joint Hilbert space is $\mathcal{H}_S \otimes \mathcal{H}_E = \mathcal{H}_2 \otimes \mathcal{H}_2$. Their Hamiltonian is

$$H = H_S \otimes \mathbb{1}_E + \mathbb{1}_S \otimes H_E + H_{\text{int}},$$

with H_{int} as their interaction. This interaction is what causes this composite system to get entangled as it evolves in time. Our model assumes that

only a single such interaction occurs at each time step, and that the environment qubit is measured and the new system state found before the next interaction takes place. Additionally, we assume that the environment has no Hamiltonian $H_E = 0$, and that all interacting environment qubits start in some inital pure state.

1.2.2 Interactions

As a general assumption of the trajectory model, the interactions we consider should be weak, meaning that they are close to the identity. To achieve this, an interaction on the form

$$H_{\text{int}} = \sum_j A_j \otimes B_j,$$

must be chosen, where each part of the tensor product is a 2×2-matrix constructed from the basis set $\{\mathbb{1}, \sigma_x, \sigma_y, \sigma_z\}$. The **A**-part acts on the Hilbert space of the system, while the **B**-part acts on the environment Hilbert space. It is then possible to parameterise the interaction, bringing it to the form

$$U(\theta) = \exp(-i\theta H_{\text{int}}) = \exp\left(-i\theta \sum_j A_j \otimes B_j\right),$$

and effectively making it a weak interaction. We later make use of this by finding the interactions linked to a master equation with the specific dynamics we want, and then expanding the parameterised version to second order in θ. This second-order expansion is then used in the successive interactions between environment and system, giving us the discrete time evolution that we want.

1.2.3 Measurements

An important property of quantum trajectories is that a measurement of the environment state after interacting with the system should be a *weak measurement*, that is, yield a small amount of information on average about the system state. Consequently, the system state is, on average, only slightly disturbed by the measurement. This allows us to monitor the system state by successively measuring environment states that have weakly interacted with the system state, hence, indirectly obtaining information about the system. Without explaining further, it should be noted that in the actual trajectories simulation, the measurements turn out to be weak because the interactions we use are weak. So the measurements we perform turns out to be similar to those we look at in this section, without us directly making them to be so.

A measurement in quantum mechanics can be described in a general way as a *positive operator valued measurement* (POVM). It requires a set of positive operators which sum to the identity

$$\sum_n E_n = \mathbb{1},$$

where for a mixed state the probability of outcome n is given by $p_n = \mathrm{Tr}(E_n\rho)$. Knowing E_n is not sufficient to determine the state after the measurement. We must also know a set of operators A_{nk} such that

$$E_n = \sum_k A_{nk}^\dagger A_{nk}.$$

Using these operators, the new mixed state can be found after a measurement outcome n as

$$\rho' = \frac{1}{p_n}\sum_k A_{nk}\rho A_{nk}^\dagger.$$

This measurement does not preserve the purity of states, unless each E_n has a single A_{nk}, in which case the new state is $|\psi'\rangle = A_n|\psi\rangle/\sqrt{p_n}$.

Now, let us look at two types of weak measurements for a two-level system. A weak measurement is in general a kind of POVM, where we parameterise the measurement operators E_n with an $\epsilon \ll 1$. The first type of weak measurement has a high probability of a small change to the state, and consequently, a low probability of a large change to the state. To obtain this behaviour the following two operators can be found

$$\begin{aligned} E_0 &\equiv |0\rangle\langle 0| + (1-\epsilon)|1\rangle\langle 1| = A_0^2, & A_0 &\equiv |0\rangle\langle 0| + \sqrt{1-\epsilon}\,|1\rangle\langle 1|, \\ E_1 &\equiv \epsilon|1\rangle\langle 1| = A_1^2, & A_1 &\equiv \sqrt{\epsilon}\,|1\rangle\langle 1|. \end{aligned}$$

Performing this POVM on a state $|\psi\rangle = \alpha|0\rangle + \beta|1\rangle$, we find the probabilities

$$\begin{aligned} p_0 &= \mathrm{Tr}(E_0|\psi\rangle\langle\psi|) = |\alpha|^2 + (1-\epsilon)|\beta|^2 = 1 - \epsilon|\beta|^2, \\ p_1 &= \mathrm{Tr}(E_1|\psi\rangle\langle\psi|) = \epsilon|\beta|^2, \end{aligned}$$

with the new states being

$$\begin{aligned} |\psi_0\rangle &= \frac{1}{\sqrt{p_0}}A_0|\psi\rangle = \frac{1}{\sqrt{p_0}}\big(\alpha|0\rangle + \beta\sqrt{1-\epsilon}\,|1\rangle\big), \\ |\psi_1\rangle &= \frac{1}{\sqrt{p_1}}A_1|\psi\rangle = \frac{1}{\sqrt{\epsilon|\beta|^2}}\big(\beta\sqrt{\epsilon}\,|1\rangle\big) = |1\rangle. \end{aligned}$$

We observe that the measurement outcome 1 greatly changes the state, but has a small probability. So on average the state will only be slightly changed in accordance with measurement outcome 0. The second type of weak measurement instead have probabilities $p_0 \approx p_1 \approx 1/2$ with both outcomes only slightly changing the state. We define the operators

$$\begin{aligned} E_0 &\equiv \left(\frac{1+\epsilon}{2}\right)|0\rangle\langle 0| + \left(\frac{1-\epsilon}{2}\right)|1\rangle\langle 1| = A_0^2, \\ E_1 &\equiv \left(\frac{1-\epsilon}{2}\right)|0\rangle\langle 0| + \left(\frac{1+\epsilon}{2}\right)|1\rangle\langle 1| = A_1^2, \\ A_0 &\equiv \sqrt{\frac{1+\epsilon}{2}}\,|0\rangle\langle 0| + \sqrt{\frac{1-\epsilon}{2}}\,|1\rangle\langle 1|, \\ A_1 &\equiv \sqrt{\frac{1-\epsilon}{2}}\,|0\rangle\langle 0| + \sqrt{\frac{1+\epsilon}{2}}\,|1\rangle\langle 1|. \end{aligned}$$

We find the probabilities

$$p_0 = \mathrm{Tr}(E_0 \left|\psi\right\rangle\!\left\langle\psi\right|) = \frac{1}{2}\big(1 + \epsilon\big(|\alpha|^2 - |\beta|^2\big)\big),$$
$$p_1 = \mathrm{Tr}(E_1 \left|\psi\right\rangle\!\left\langle\psi\right|) = \frac{1}{2}\big(1 + \epsilon\big(|\beta|^2 - |\alpha|^2\big)\big),$$

with the new states being

$$\left|\psi_0\right\rangle = \frac{1}{\sqrt{p_0}} A_0 \left|\psi\right\rangle \approx \alpha\big(1 + \epsilon|\beta|^2\big)\left|0\right\rangle + \beta\big(1 - \epsilon|\alpha|^2\big)\left|0\right\rangle,$$
$$\left|\psi_1\right\rangle = \frac{1}{\sqrt{p_1}} A_1 \left|\psi\right\rangle \approx \alpha\big(1 - \epsilon|\beta|^2\big)\left|0\right\rangle + \beta\big(1 + \epsilon|\alpha|^2\big)\left|0\right\rangle.$$

With ϵ sufficiently small, the trajectories evolve in a diffusive way, where the measurement outcomes are almost equally likely and the changes to the system state are small. The first type of measurement on the other hand will give us trajectories which have some large jumps in their evolution. It should be noted that these measurement schemes are not directly applied in our method. Rather, the weak interactions that we define for the trajectories simulation, and the basis in which we choose to measure the environment, will give us measurements corresponding to either diffusive measurements or measurements with jumps.

1.2.4 Master equation

The time evolution of a density matrix is found by solving the Lindblad master equation. For an introduction to this, see reference [15].

$$\frac{\mathrm{d}\rho}{\mathrm{d}t} = -\frac{i}{\hbar}[H_S, \rho] + \sum_k \left[L_k \rho L_k^\dagger - \frac{1}{2}\Big(L_k^\dagger L_k \rho + \rho L_k^\dagger L_k\Big)\right] \tag{1.4}$$

Here, H_S is the system Hamiltonian and L_k Lindblad operators. Now, we want to relate the discrete time evolution of QTT to the master equation. By doing so we can find how our choice of interaction and environment specifies a certain master equation, and importantly the corresponding Lindblad operators. Let us first assume some general unitary interaction U acting on the composite Hilbert space $\mathcal{H}_S \otimes \mathcal{H}_E$, where S denotes the system space, and E denotes the environment state. We may write this as a sum of product operators. As before, we have the interaction on the form

$$H_{\mathrm{int}} = \sum_j A_j \otimes B_j,$$

with $\mathbf{A}$ acting on the system, and $\mathbf{B}$ on the environment. Applying this unitary transformation on the initial composite system state $\left|\Psi\right\rangle = \left|\psi\right\rangle \otimes \left|E\right\rangle$, where $\left|\psi\right\rangle$ is the system state and $\left|E\right\rangle$ is the environment state, gives us a

new density matrix for the system ρ'_S.

$$\begin{aligned}\rho'_S &= \mathrm{Tr}_{\mathrm{env}}\left[H_{\mathrm{int}}\left|\Psi\right\rangle\left\langle\Psi\right|H_{\mathrm{int}}^{\dagger}\right] \\ &= \sum_{j,j'}\mathrm{Tr}_{\mathrm{env}}\left[\left(A_j\left|\psi\right\rangle\left\langle\psi\right|A_{j'}^{\dagger}\right)\otimes\left(B_j\left|E\right\rangle\left\langle E\right|B_{j'}^{\dagger}\right)\right] \\ &= \sum_{j,j'}A_j\left|\psi\right\rangle\left\langle\psi\right|A_{j'}^{\dagger}\left\langle E\right|B_jB_{j'}^{\dagger}\left|E\right\rangle \end{aligned} \tag{1.5}$$

From this we find the self-adjoint matrix $M_{j,j'} \equiv \langle E| B_j B_{j'} |E\rangle$. This matrix gives us a set of orthonormal eigenvectors $\boldsymbol{\mu}_k$ with real eigenvalues λ_k such that

$$\sum_{j'} = M_{jj'}\mu_{kj'} = \lambda_k\mu_{kj} \implies M_{jj'} = \sum_k \lambda_k\mu_{kj}\mu^*_{kj'}.$$

Note that the elements of the eigenvectors $\boldsymbol{\mu}_k$ are indexed by j. Using this we may define a new set of operators O_k,

$$O_k \equiv \sqrt{\lambda_k}\sum_j \mu_{kj}A_j,$$

that lets us simplify expression (1.5). We then get it on the form

$$\rho'_S = \mathrm{Tr}_{\mathrm{env}}\left[H_{\mathrm{int}}\left|\Psi\right\rangle\left\langle\Psi\right|H_{\mathrm{int}}^{\dagger}\right] = \sum_k O_k\left|\psi\right\rangle\left\langle\psi\right|O_k^{\dagger}$$

Then, after n interactions between system and environment we have

$$\rho_S^{(n)} = \sum_{k_1\ldots k_n} O_{k_n}\ldots O_{k_1}\left|\psi\right\rangle\left\langle\psi\right|O_{k_1}^{\dagger}\ldots O_{k_n}^{\dagger}.$$

As we can see, this is the expected behavior of a discrete master equation.

Next, we will consider the case where we instead have some unitary operator U, close to the identity. We can achieve this by parameterising the interaction H_{int} with some real number $\theta \ll 1$, so that we get it on the form:

$$U(\theta) = \exp(-i\theta H_{\mathrm{int}}) = \exp\left\{-i\theta\sum_j A_j\otimes B_j\right\}.$$

If we then expand the evolved density matrix ρ'_S to second order in θ using this operator we find:

$$\begin{aligned}\rho'_S &= \mathrm{Tr}_{\mathrm{env}}\left[U(\theta)\left|\Psi\right\rangle\left\langle\Psi\right|U(\theta)^{\dagger}\right] \\ &\approx \left|\psi\right\rangle\left\langle\psi\right| - i\theta\sum_j\left[A_j,\left|\psi\right\rangle\left\langle\psi\right|\right]\left\langle E\right|B_j\left|E\right\rangle + \frac{\theta^2}{2}\sum_{jj'}\left\langle E\right|B_{j'}B_j\left|E\right\rangle \\ &\times\left(2A_j\left|\psi\right\rangle\left\langle\psi\right|A_{j'} - A_jA_{j'}\left|\psi\right\rangle\left\langle\psi\right| - \left|\psi\right\rangle\left\langle\psi\right|A_jA_{j'}\right)\end{aligned} \tag{1.6}$$

The full derivation of the above result is not essential to follow the argument, but can be found in the appendix. Furthermore, we can make the simplifying assumption that the first-order term vanishes:

$$\sum_j A_j\left\langle E\right|B_j\left|E\right\rangle = 0, \tag{1.7}$$

which is easily achieved by subtracting any non vanishing terms in the sum from our unitary operator as a correction to the exponentiated matrix. As shown for equation (1.5) we may define the self-adjoint matrix $M_{jj'}$,

$$M_{jj'} = \langle E| B_j B_{j'} |E\rangle ,$$

that has orthonormal eigenvectors $\boldsymbol{\mu}_k$ and real eigenvalues λ_k. Additionally, we impose a duration δt for the interaction so that equation (1.6) can approximate the time derivative of the master equation (1.4). Having this, we can define operators

$$L_k = \sqrt{\frac{\theta^2\lambda_k}{\delta t}} \sum_j \mu_{kj} A_j = \sqrt{\frac{\theta^2\lambda_k}{\delta t}} \alpha_k. \tag{1.8}$$

Writing equation (1.6) in terms of these operators then gives us

$$\begin{aligned} \frac{\rho' - \rho}{\delta t} &= \sum_k \left[L_k \rho L_k^\dagger - \frac{1}{2} L_k^\dagger L_k \rho - \frac{1}{2} \rho L_k^\dagger L_k \right], \\ &= \left(\frac{\theta^2}{\delta t} \right) \sum_k \lambda_k \left[\alpha_k \rho \alpha_k^\dagger - \frac{1}{2} \alpha_k^\dagger \alpha_k \rho - \frac{1}{2} \rho \alpha_k^\dagger \alpha_k \right], \end{aligned} \tag{1.9}$$

which has the form of the master equation with no effective Hamiltonian.

Chapter 2

Method

Having covered the necessary background material, we now move on to explain how quantum trajectory theory can be used to find frequency synchronisation in a dissipative two-level system. The goal of this chapter is to thoroughly explain every step involved when constructing quantum trajectory simulations, and to demonstrate the validity of our results.

The first section covers how to find interactions between system and environment that results in the dissipative behavior necessary to study synchronisation. This follows closely from the background material in section 1.2.4. Having identified the interactions, we then show how statistics for the transition rates can be included into our model by modifying the interaction strength parameter θ. We then demonstrate how the new system state is determined after the interaction, by measuring the environment state.

After the basic method is covered, the structure and use of the numerical model is explained. To test the method's validity, we compare results from QTT simulations with the master equation. Figures of single trajectories and their corresponding density matrix, represented on the Bloch sphere, are shown. Additionally, we compare QTT simulations with different temperatures to the master equation, testing the statistics of the model.

The final part explains how a system Hamiltonian can be applied to the simulations, along with figures to show the validity of the implementation. Finally, the method for calculating angular frequencies for individual trajectories, and thereby measuring the angular frequency of the system, will be covered. This enables us to study how the synchronisation to an external signal changes with detuning.

2.1 Developing a model using quantum trajectory theory

2.1.1 Deriving QTT interactions

To make our quantum trajectory simulations reproduce the behavior of a dissipative system, like the one studied in [2], we need to find interactions corresponding to the operators of the Lindblad master equation describing such a system. A description of how to find Lindblad operators from these types of interactions can be found in section 1.2.4. The relationship between interactions and Lindblad operators is of a kind that we are unable to solve directly. Therefore, we approach the problem by identifying the properties of the Lindblad operators, and then simplifying to make an ansatz of the correct interaction. The interactions are of the form

$$H_{\text{int}} = \sum_j A_j \otimes B_j,$$

where **A** operates on the system state, and **B** on the environment. Their basis matrices are $\{\mathbb{1}, \sigma_x, \sigma_y, \sigma_z\}$. Our goal is to find some H_{int} corresponding to the absorption and emission Lindblad operators

$$L_+ = \gamma_+ |1\rangle\langle 0| = \gamma_+\sigma_+, \quad L_- = \gamma_- |0\rangle\langle 1| = \gamma_-\sigma_-, \quad \sigma_\pm = \frac{1}{2}(\sigma_x \pm i\sigma_y).$$

In the next section we show how the γ-factors, which correspond to the transition rates, can be calculated to suit our model. For now, we focus on finding interactions that give the Lindblad operators the correct matrix representation. They should in our case be represented by the raising and lowering operators $\sigma_\pm$. The Lindblad operators correspond to the choice of interaction by equation (1.8). Repeated here for convenience:

$$L_k = \sqrt{\frac{\theta^2\lambda_k}{\delta t}} \sum_j \mu_{kj} A_j = \gamma\sqrt{\lambda_k}\alpha_k, \quad \gamma = \sqrt{\frac{\theta^2}{\delta t}}, \quad \alpha_k = \sum_j \mu_{kj} A_j,$$

where λ_k are the eigenvalues and $\boldsymbol{\mu}_k$ the eigenvectors of the self-adjoint matrix $M_{jj'}$. The self-adjoint matrix is constructed from the environment state and **B** by $M_{jj'} = \langle E| B_j B_{j'} |E\rangle$. The above equation suggests that a single H_{int} could be identified to directly give us two operators for the master equation. However, we make the assumption that two interactions can be applied in the trajectories simulation. The simulation will then work by alternating evenly between the two interactions, so that for the first time step the interaction corresponding to L_+ is used, and then the interaction corresponding to L_- for the next time step, and so on. This assumption is not necessary, there should exist a more complicated interaction which directly gives us two Lindblad operators. The assumption is a convenient way of simplifying the procedure. Therefore, we are looking for two $H_{\text{int}\pm}$ each corresponding separately to $L_\pm$.

We begin by observing that we may choose

$$A_1 = \sigma_x, \quad A_2 = \sigma_y,$$

such that

$$\alpha_k = \sum_j \mu_{kj} A_j = \mu_{k1}\sigma_x + \mu_{k2}\sigma_y.$$

If $M_{jj'}$ has a single nonvanishing eigenvalue, the problem is reduced to identifying a $\mathbf{B}$ so that $\boldsymbol{\mu} = (1, i)$. The sign of μ_2 is unimportant because we are free to change the sign of A_2. Furthermore, expressing $M_{jj'}$ explicitly, we have

$$M_{jj'} = \begin{pmatrix} \langle E| B_1^2 |E\rangle & \langle E| B_1 B_2 |E\rangle \\ \langle E| B_2 B_1 |E\rangle & \langle E| B_2^2 |E\rangle \end{pmatrix}.$$

We can limit $\mathbf{B}$ to only contain basis matrices, hence we have the property that $B_j^2 = \mathbb{1}$, and so all diagonal elements will be 1. From this we observe that a matrix with the properties we are looking for is

$$M = \begin{pmatrix} 1 & -i \\ i & 1 \end{pmatrix},$$

with $\boldsymbol{\mu} = (1, i)$ and $\lambda = 2$. We then see that the problem can be solved by identifying B_1 and B_2 so that

$$\langle E| B_1 B_2 |E\rangle = i.$$

Now, recall that the Pauli matrices satisfy

$$\sigma_i \sigma_j = \delta_{ij}\mathbb{1} + i\epsilon_{ijk}\sigma_k, \text{ with } \{\sigma_1 = \sigma_x, \sigma_2 = \sigma_y, \sigma_3 = \sigma_z\}.$$

(Here δ_{ij} is the Kronecker delta and ϵ_{ijk} is the Levi-Civita.) From the antisymmetry of ϵ_{ijk} we observe that

$$\langle E| B_1 B_2 |E\rangle = +i \implies \langle E| B_2 B_1 |E\rangle = -i.$$

In our case, we may take the assumption in equation (1.7) to imply that $\langle E| B_j |E\rangle = 0$ for $j = 1$ and 2. In doing so, we make the assumption more limiting than it has to be, but this is a helpful restriction on $\mathbf{B}$ because it excludes the basis matrices $\{\mathbb{1}, \sigma_E\}$, as these would give nonvanishing inner products. The notation σ_E means that, if we choose $|E\rangle$ in the z-basis $\{|0\rangle, |1\rangle\}$ we have $\sigma_E = \sigma_z$. By this last step, we have more or less uniquely determined B_1 and B_2 for any given $|E\rangle$.

Now, we look at the case of having the environment in the z-basis $|E\rangle = |0\rangle$. Our choice for $\mathbf{B}$ is then

$$B_1 = \sigma_x, \quad B_2 = \sigma_y,$$

since the only other option is rearranging the order. (Which simply amounts to a sign change.) We then get the self-adjoint matrix

$$M_{jj'} = \begin{pmatrix} \langle 0| \sigma_x^2 |0\rangle & \langle 0| \sigma_y \sigma_x |0\rangle \\ \langle 0| \sigma_x \sigma_y |0\rangle & \langle 0| \sigma_y^2 |0\rangle \end{pmatrix} = \begin{pmatrix} 1 & -i \\ i & 1 \end{pmatrix}.$$

Hence, we get $\boldsymbol{\mu} = (1, i)$ with $\lambda = 2$ and the resulting Lindblad operator is

$$L_+ = \sqrt{\frac{\theta^2}{\delta t}}\sqrt{2}(\sigma_x + i\sigma_y) = \sqrt{\frac{\theta^2}{\delta t}} 2\sqrt{2}\sigma_+.$$

Thus, we have found the interaction corresponding to the absorption operator in the master equation. We then swap the sign of A_2 which then directly gives us the emission operator. For convenience, we include a factor $1/4$ on both A_1 and A_2, thus the resulting interactions found for $|E\rangle = |0\rangle$ are

$$H_{\text{int}}+ = \frac{1}{4}(\sigma_x \otimes \sigma_x + \sigma_y \otimes \sigma_y),$$
$$H_{\text{int}}- = \frac{1}{4}(\sigma_x \otimes \sigma_x - \sigma_y \otimes \sigma_y).$$

And the corresponding Lindblad operators are

$$L_+ = \sqrt{\frac{\theta^2}{2\delta t}}\sigma_+, \quad L_- = \sqrt{\frac{\theta^2}{2\delta t}}\sigma_-.$$

The interaction we found above is then parameterised and exponentiated so that we obtain weak interactions on the form

$$U(\theta) = \exp\left\{ -i\theta \sum_j A_j \otimes B_j \right\} = \exp\{-i\theta H_{\text{int}}\}.$$

In simulating QTT, we expand these interaction operators to second order in θ for $\theta \ll 1$:

$$U(\theta) \approx \mathbb{1} - i\theta H_{\text{int}} - \frac{\theta^2}{2} H_{\text{int}}^2.$$

2.1.2 Time evolution and statistics

In this subsection we will cover the general scheme for simulating QTT. We start with some initial pure state for the system $|\psi_0\rangle$. For every time step δt, the system state and the environment bit is described by the product state $|\Psi\rangle = |\psi\rangle \otimes |E\rangle$, which we evolve using (a second-order expansion of) a weak interaction $U(\theta)$. We then perform a measurement of the environment qubit, where we are free to choose the basis for the measurement. This will be discussed further in the next section. After the measurement is taken we are left with a new system state $|\psi'\rangle$ and the same scheme is then repeated N times.

In the previous section we showed how to derive interactions corresponding to absorption and emission. Therefore, we have two weak interactions $U_\pm(\theta)$ that we use to evolve the system. As mentioned in the previous section, a simple way of achieving this is by alternating between the two interactions, switching between $U_+(\theta)$ and $U_-(\theta)$ every time step. Additionally, we want the strength of the weak interactions to be scaled with the absorption and emission rates $\Gamma_\pm$. These rates should in turn be determined by the energy or temperature T of the system. The temperature dependence can be found using some simple statistics. Since we have a two-level system the energy is $\Delta E = E_1 - E_0$, where E_0 is the energy of the ground state and E_1 of the excited state. This gives us the partition function and probabilities

$$Z = e^{-\beta E_0} + e^{-\beta E_1}, \quad p_0 = \frac{1}{Z} e^{-\beta E_0}, \quad p_1 = \frac{1}{Z} e^{-\beta E_1}.$$

Where $\beta = 1/k_B T$, k_B is the Boltzmann constant and T is the temperature of the system. The absorption and emission rates can be related to these probabilities by

$$\frac{\Gamma_-}{\Gamma_+} = \frac{p_0}{p_1} = \frac{e^{-\beta E_0}}{e^{-\beta E_1}} = e^{\beta \Delta E}. \tag{2.1}$$

Now, we assume the rates are given by the Bose-Einstein distribution

$$n = \frac{1}{e^{\beta \Delta E} - 1}, \quad \Gamma_+ = n, \quad \Gamma_- = n + 1.$$

This gives us the explicit rates

$$\Gamma_+ = \frac{1}{e^{\beta \Delta E} - 1}, \quad \Gamma_- = \frac{e^{\beta \Delta E}}{e^{\beta \Delta E} - 1},$$

which satisfies relation 2.1. For our numerical simulations we will simplify by using $k_B = 1$, but keeping the temperature as a parameter.

Having found expressions for the rates, we then scale the interaction strength parameter θ for the weak interactions. This leaves us with two interaction strength parameters, one for the absorption and one for emission:

$$\theta_+ = \sqrt{\Gamma_+}\theta, \quad \theta_- = \sqrt{\Gamma_-}\theta$$

Having this, we get the Lindblad operators

$$L_\pm = \sqrt{\frac{\theta_\pm^2}{2\delta t}}\sigma_\pm = \sqrt{\frac{\Gamma_\pm \theta^2}{2\delta t}}\sigma_\pm.$$

Inserting these into the master equation, we get

$$\begin{aligned}\frac{\rho' - \rho}{\delta t} = \frac{\theta^2}{\delta t}\Bigg(&\frac{\Gamma_+}{2}\left[\sigma_+\rho\sigma_+^\dagger - \frac{1}{2}\sigma_+^\dagger\sigma_+\rho - \frac{1}{2}\rho\sigma_+^\dagger\sigma_+\right] \\ &+ \frac{\Gamma_-}{2}\left[\sigma_-\rho\sigma_-^\dagger - \frac{1}{2}\sigma_-^\dagger\sigma_-\rho - \frac{1}{2}\rho\sigma_-^\dagger\sigma_-\right]\Bigg),\end{aligned}$$

which is of the same form as the approximated master equation (1.9) with the addition of the transition rates.

2.1.3 Measurements

Here we explain the measurement part of the QTT time evolution scheme that was described in the previous section. We aim to find the new system state $|\psi'\rangle$ after the weak interaction with the environment bit. This is found by measuring the environment bit in the entangled state, hence we need to determine probabilities for the measurement outcomes. After the weak interaction has been applied to the product state we get the new entangled state $|\Psi'\rangle$. This can be expressed on a general form as

$$\begin{aligned}\left|\Psi'\right\rangle &= c_{00}\left|00\right\rangle + c_{01}\left|01\right\rangle + c_{10}\left|10\right\rangle + c_{11}\left|11\right\rangle \\ &= \left(c_{00}\left|0\right\rangle + c_{10}\left|1\right\rangle\right) \otimes \left|0\right\rangle + \left(c_{01}\left|0\right\rangle + c_{11}\left|1\right\rangle\right) \otimes \left|1\right\rangle.\end{aligned}$$

In the following, assume that the environment qubit is measured in the x-basis $\{|x_+\rangle, |x_-\rangle\}$. The first step is to rewrite the above state with the environment qubit in this basis,

$$\begin{aligned}
\left|\Psi'\right\rangle &= (c_{00}\left|0\right\rangle + c_{10}\left|1\right\rangle) \otimes \frac{1}{\sqrt{2}}(|x_+\rangle + |x_-\rangle) \\
&\quad + (c_{01}\left|0\right\rangle + c_{11}\left|1\right\rangle) \otimes \frac{1}{\sqrt{2}}(|x_+\rangle - |x_-\rangle), \\
&= \frac{1}{\sqrt{2}}\{(c_{00}+c_{01})\left|0\right\rangle + (c_{10}+c_{11})\left|1\right\rangle\} \otimes |x_+\rangle \\
&\quad + \frac{1}{\sqrt{2}}\{(c_{00}-c_{01})\left|0\right\rangle + (c_{10}-c_{11})\left|1\right\rangle\} \otimes |x_-\rangle\,, \\
&= \left|\psi'_+\right\rangle \otimes |x_+\rangle + \left|\psi'_-\right\rangle \otimes |x_-\rangle\,.
\end{aligned}$$

The notation might seem ambiguous, but $\left|\psi'_\pm\right\rangle$ denotes the system states resulting from measuring the environment state in either $|x_+\rangle$ or $|x_-\rangle$, and importantly have nothing to do with absorption and emission. To find the probabilities of measuring the environment qubit in either of the measurement basis states we find the environment density matrix by tracing over the system.

$$\begin{aligned}
\rho'_E &= \mathrm{Tr}_{sys}\left[\left|\Psi'\right\rangle\left\langle\Psi'\right|\right] \\
&= \sum_i \Big(\left\langle i\middle|\psi'_+\right\rangle \left\langle\psi'_+\middle|i\right\rangle |x_+\rangle\langle x_+| + \left\langle i\middle|\psi'_+\right\rangle \left\langle\psi'_-\middle|i\right\rangle |x_+\rangle\langle x_-| \\
&\quad + \left\langle i\middle|\psi'_-\right\rangle \left\langle\psi'_+\middle|i\right\rangle |x_-\rangle\langle x_+| + \left\langle i\middle|\psi'_-\right\rangle \left\langle\psi'_-\middle|i\right\rangle |x_-\rangle\langle x_-| \Big), \\
&= \sum_i \Big(\left\langle\psi'_+\middle|i\right\rangle \left\langle i\middle|\psi'_+\right\rangle |x_+\rangle\langle x_+| + \dots \Big), \\
&= \left\langle\psi'_+\middle|\psi'_+\right\rangle |x_+\rangle\langle x_+| + \cdots + \left\langle\psi'_-\middle|\psi'_-\right\rangle |x_-\rangle\langle x_-|\,.
\end{aligned}$$

Now, having found the density matrix of the environment the probabilities are the coefficients we get from the system state after performing the trace. Thus, we identify the probabilities as

$$p_+ = \left\langle\psi'_+\middle|\psi'_+\right\rangle, \quad p_- = \left\langle\psi'_-\middle|\psi'_-\right\rangle,$$

with corresponding system states

$$\left|\psi'\right\rangle = \begin{cases} \frac{1}{\sqrt{p_+}}\left|\psi'_+\right\rangle, & \text{environment measured in } |x_+\rangle \text{ with probability } p_+, \\ \frac{1}{\sqrt{p_-}}\left|\psi'_-\right\rangle, & \text{environment measured in } |x_-\rangle \text{ with probability } p_-. \end{cases}$$

The updated system states and measurement probabilities for the z and y basis are found with the same method. The entangled state is expressed

with the environment in the measurement basis, and so for z and y we have

$$\begin{aligned}\left|\Psi'_z\right\rangle &= \{c_{00}\left|0\right\rangle + c_{10}\left|1\right\rangle\} \otimes \left|0\right\rangle \\ &\quad + \{c_{01}\left|0\right\rangle + c_{11}\left|1\right\rangle\} \otimes \left|1\right\rangle, \\ \left|\Psi'_y\right\rangle &= \frac{1}{\sqrt{2}}\{(c_{00} - ic_{01})\left|0\right\rangle + (c_{10} - ic_{11})\left|1\right\rangle\} \otimes \left|y_+\right\rangle \\ &\quad + \frac{1}{\sqrt{2}}\{(c_{00} + ic_{01})\left|0\right\rangle + (c_{10} + ic_{11})\left|1\right\rangle\} \otimes \left|y_-\right\rangle.\end{aligned}$$

2.2 Trajectories simulation and testing

2.2.1 Numerical simulation of the model

In the previous sections we demonstrated the time evolution of a system state $|\psi(t)\rangle$ using quantum trajectory theory. To test the model, we implement it numerically and use a Monte Carlo method. This entails simulating a number of trajectories, calculating the density matrix for each, and then take the mean of these density matrices. If our model works as intended, this should then approximate the solution given by the Lindblad master equation. To allow the reader to follow the figures and tests of the model, it is helpful to go through the structure of the numerical implementation.

We start with the initial system state $|\psi_0\rangle$ and construct the product state of the initial system and the environment by $|\Psi\rangle = |\psi_0\rangle \otimes |E\rangle$. Next, the system state and the environment qubit interact, which we implement by applying the weak interaction operators $U_\pm(\theta)$, expanded to second order in θ. To get both the absorption and emission behaviour, we alternate between using $U_+(\theta)$ and $U_-(\theta)$ each time step. This gives us an updated entangled state $|\Psi'\rangle$. The final step is to compute the probabilities of measuring the environment bit in either $\{|f_+\rangle, |f_-\rangle\}$, for some basis f that we choose. The new system state $|\psi_1\rangle$ is then chosen by using a random number generator to determine the measurement outcome. This process is then repeated N times, until the whole trajectory of the system state,

$$|\psi(t)\rangle = (|\psi_0\rangle, |\psi_1\rangle \quad \dots \quad |\psi_{N-1}\rangle),$$

has been determined. Using this scheme we then simulate S trajectories, and for each we find the density matrix

$$\rho_j(t) = |\psi_j(t)\rangle \langle\psi_j(t)|.$$

Taking the mean of these density matrices we then find

$$\rho(t) = \frac{1}{S}\sum_{j=1}^{S} \rho_j(t),$$

which approximates the solution found using the Lindblad master equation.

There are several key elements and parameters used in the simulations. For clarity, we repeat them here. The first element we need to choose before starting a QTT simulation is the environment qubit $|E\rangle$. The state of

the environment, as we saw in section 2.1.1, affects the form of the weak interactions that we use in the simulation. Secondly, we need to choose $\theta \ll 1$ to ensure that the interactions are weak. Additionally, a choice must be made for the time step δt and the number of time steps N. As we are approximating the master equation (1.9), we must choose δ sufficiently small for the approximation to be valid. Consequently, we must choose N sufficiently large to allow us to observe the time evolution. The number of trajectories S determines how exact the approximation follows the time evolution of the master equation. Naturally, increasing S directly increases the time it takes to complete the simulation. Finally, we need to initialise the simulation with some temperature T and an initial system state $|\psi_0\rangle$.

2.2.2 Comparison with Lindblad

Trajectories are simulated as described in the previous section to find the density matrix approximation of the master equation. To visualise the results, we compare the Bloch vector components for both the QTT and the master equation solution. Recall, a density matrix ρ can be described using the Bloch vector $\mathbf{r}$ as

$$\rho = \frac{1}{2}(\mathbb{1} + \mathbf{r} \cdot \sigma), \quad \sigma = (\sigma_x, \sigma_y, \sigma_z).$$

The density matrix can be expressed in terms of the vector components as

$$\rho = \frac{1}{2}\begin{pmatrix} 1 + r_z & r_x - ir_y \\ r_x + ir_y & 1 - r_z \end{pmatrix},$$

where the components are found from

$$\begin{aligned} r_x &= \rho_{12} + \rho_{21}, \\ r_y &= i(\rho_{12} - \rho_{21}), \\ r_z &= \rho_{11} - \rho_{22}. \end{aligned}$$

Testing numerically implemented methods against known equations is always good practice. Comparing our model to the Lindblad master equation should therefore be a convincing way of proving its validity. All master equation results were obtained numerically, using the `QuTiP` (Quantum Toolbox in Python) function `mesolve`.[16] The first simulations we present in this section were carried out with the initial system state as $|\psi_0\rangle = |x_+\rangle$, the environment as $|E\rangle = |0\rangle$ and the measurements are made in the x-basis. Additionally, the following parameters were used: $\theta = 0.01$, $\delta t = 0.01$, $T = 0.5$, and $N = 2 \times 10^5$. As a test of the accuracy of the method, separate simulations computing $S = 64$ and $S = 512$ trajectories were carried out. The comparison is presented in figure 2.1. We clearly observe that the simulation produces accurate results, even for relatively few trajectories. Increasing the amounts of trajectories has the expected effect of further reducing the noise of the simulation results.

To further illuminate the behaviour of the simulated trajectories we plot a few samples on the Bloch sphere. Using the same conditions as in section

figure 2.1. Six samples are presented in figure 2.2. We observe that the behaviour of the individual trajectories are clearly diffusive, similar to what was explained for the second positive operator valued measurement in section 1.2.3. Additionally, three simulations with initial states $|1\rangle$, $|x_+\rangle$ and $|y_-\rangle$, are shown on the Bloch sphere in figure 2.3. These results suggest the model is working independently of the chosen initial state.

Comparing a set of simulations with varying temperature to the master equation, to test that our statistics are giving results with the behaviour we expect. The behaviour indicates that lowering the temperature takes the r_z component closer to 1, meaning the system state approaches $|0\rangle$. Meanwhile higher temperatures should lie closer to the center of the Bloch sphere, $\mathbf{r} = (0, 0, 0)$, which is the maximally mixed state. The temperatures chosen were $T = 0.2, 0.4, 0.6$ and 0.8, and the results are presented in figure 2.4. We observe a strong correlation between lowering the temperature, and reducing the noise of the system.

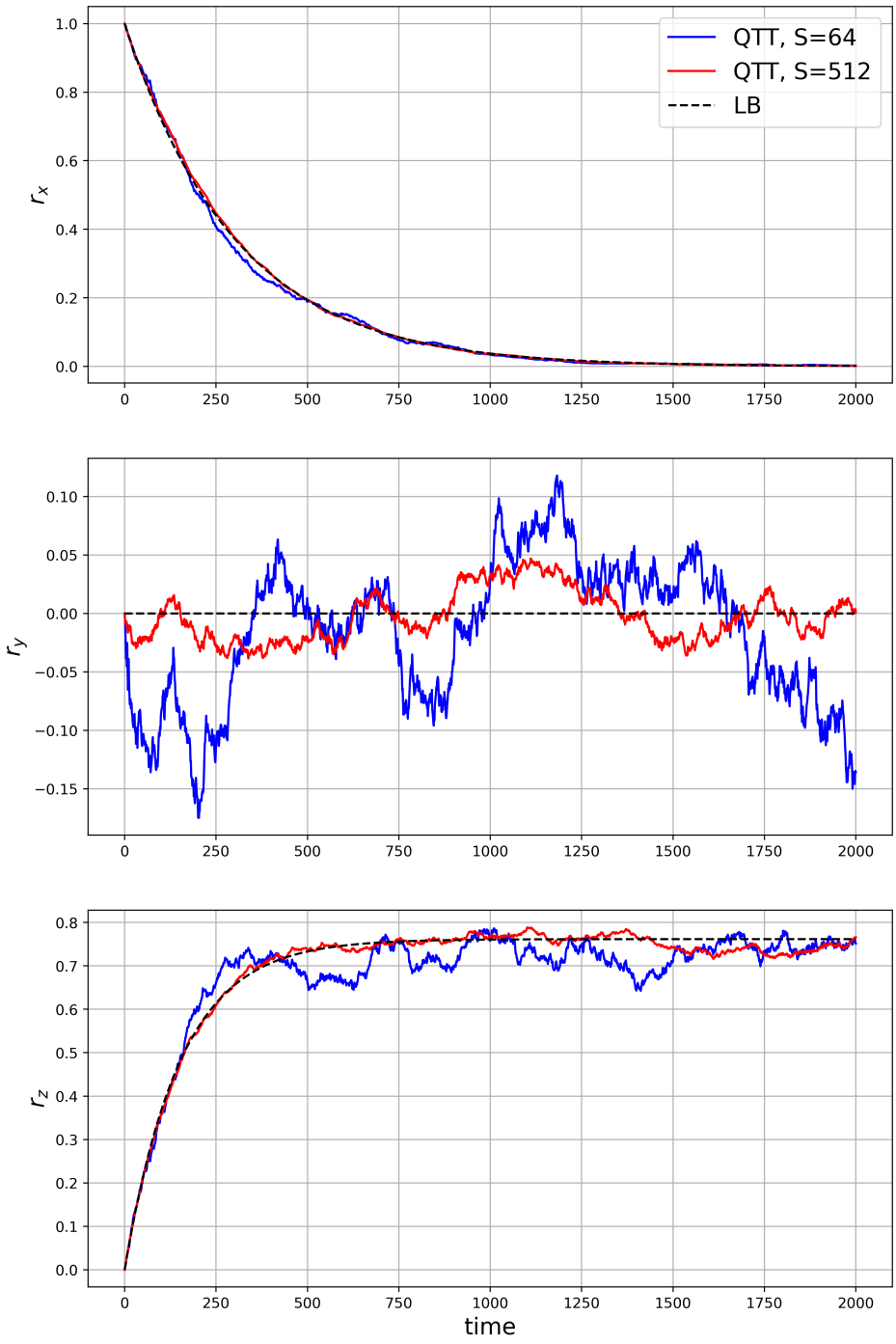

Figure 2.1: Figure comparing the Bloch vector components of the quantum trajectories model, with the solutions given by the Lindblad master equation. The trajectories were simulated using $|E\rangle = |0\rangle$, $|\psi_0\rangle = |x_+\rangle$ and measurements in the x-basis. The following parameters were used in this figure: interaction strength $\theta = 0.01$, time step $\delta t = 0.01$, and temperature $T = 0.5$. The blue QTT simulation used $S = 64$, while the red used $S = 512$.

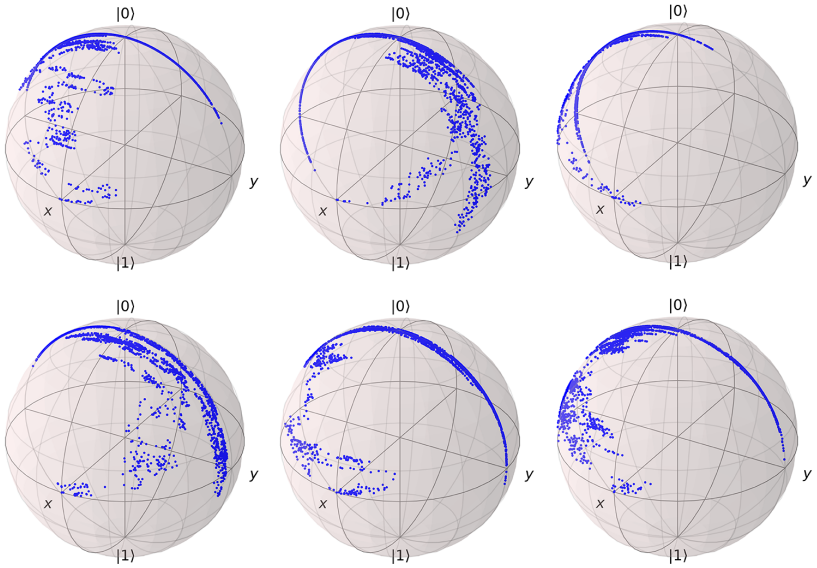

Figure 2.2: Samples of single trajectories represented on the Bloch sphere. The state is plotted every 100 time step. The initial state is $|\psi_0\rangle = |x_+\rangle$, same as the blue result in figure 2.3. Parameters for the trajectories are the same as in figure 2.1

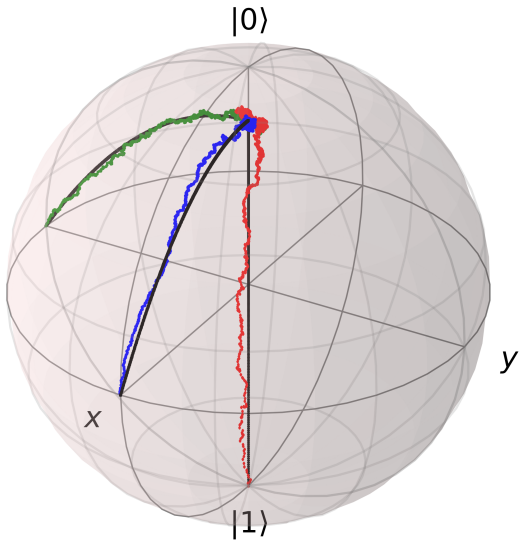

Figure 2.3: Bloch vectors of three different initial states represented on the Bloch sphere. The trajectories simulation presented in figure 2.1 is represented in blue. Two additional simulations with initial states $|1\rangle$ and $|y_-\rangle$ are represented in red and green, respectively. The master equation solution is represented in black. The parameters, environment state and measurement basis used were the same as in figure 2.1

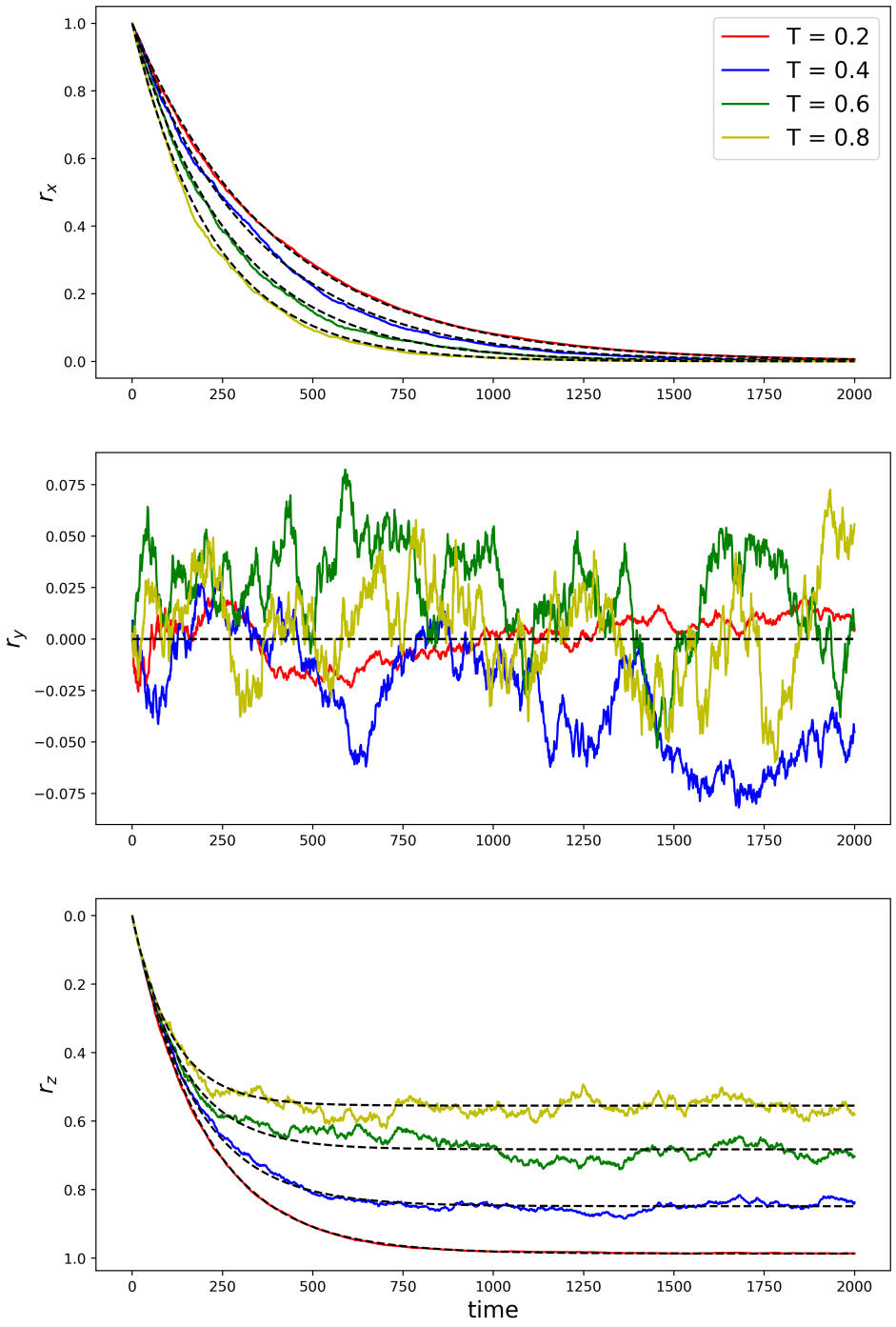

Figure 2.4: Trajectories simulated with temperatures $T = 0.2, 0.4, 0.6, 0.8$. The parameters, environment and measurement basis are the same as in 2.1, with $S = 256$, and for several temperatures.

2.3 Synchronisation with external signal

2.3.1 Applying a classical drive signal Hamiltonian

The goal of our model is to study frequency synchronisation, and to do so we require that the system evolves with an effective Hamiltonian. As was done in [2] and covered in section 1.1.2, we use the classical drive Hamiltonian. This Hamiltonian acts as an external signal with frequency ω and strength ϵ. In the rotating wave approximation, the Hamiltonian is given by

$$H_{\text{signal}} = i\hbar\frac{\epsilon}{2}\big(e^{i\omega t}\sigma_- - e^{-i\omega t}\sigma_+\big).$$

To simplify calculations we use $\hbar = 1$, unless otherwise stated. We transform the system to a reference frame rotating with the signal frequency ω by using the transformation

$$T_\omega = \exp\Big\{i\frac{\omega}{2}\sigma_z t\Big\}.$$

By doing so, we obtain the system Hamiltonian

$$H_{\text{sys}} = \frac{\Delta}{2}\sigma_z + \frac{\epsilon}{2}\sigma_y, \tag{2.2}$$

where we have introduced $\Delta = \omega_0 - \omega$, ω_0 as the system frequency. This Hamiltonian is on an ideal form for studying synchronisation because it lets us vary the detuning Δ and the strength of the external signal ϵ.

The system Hamiltonian can then be implemented in a similar way to the weak interactions $U(\theta)$ described in section 2.2.1. In the standard formalism the time evolution of a state is described by the Schrödinger equation

$$\frac{\mathrm{d}}{\mathrm{d}t}\left|\psi\right\rangle = -iH(t)\left|\psi\right\rangle.$$

For numerical simulations we treat time as a discrete variable δt and find the time evolution as a series of unitary operations on the system state. For a $\delta t \ll 1$ one can find unitary operators on the form

$$U = \exp\{-i\delta t H\} \approx \mathbb{1} - i\delta t H - \frac{\delta t^2}{2}H^2 + \ldots,$$

which then can be applied for each time step to get

$$\left|\psi_N\right\rangle = U_N U_{N-1}\ldots U_1\left|\psi_0\right\rangle.$$

In the simulation scheme we apply the unitary Hamiltonian to the system state for every time step after the measurement outcome is resolved. To ensure that the addition of a system Hamiltonian is compatible with the trajectories simulation we once again compare the results to the master equation. The comparison is presented in figure 2.5. We observe that the Bloch vector clearly follows the master equation solution, although with some noise. Additionally, we observe that the stationary solution is reached after approximately 1500 time units. Since we are going to be measuring the average frequency of the stationary solution of the Bloch vector, we will need to run each trajectory for this time before measuring the frequencies.

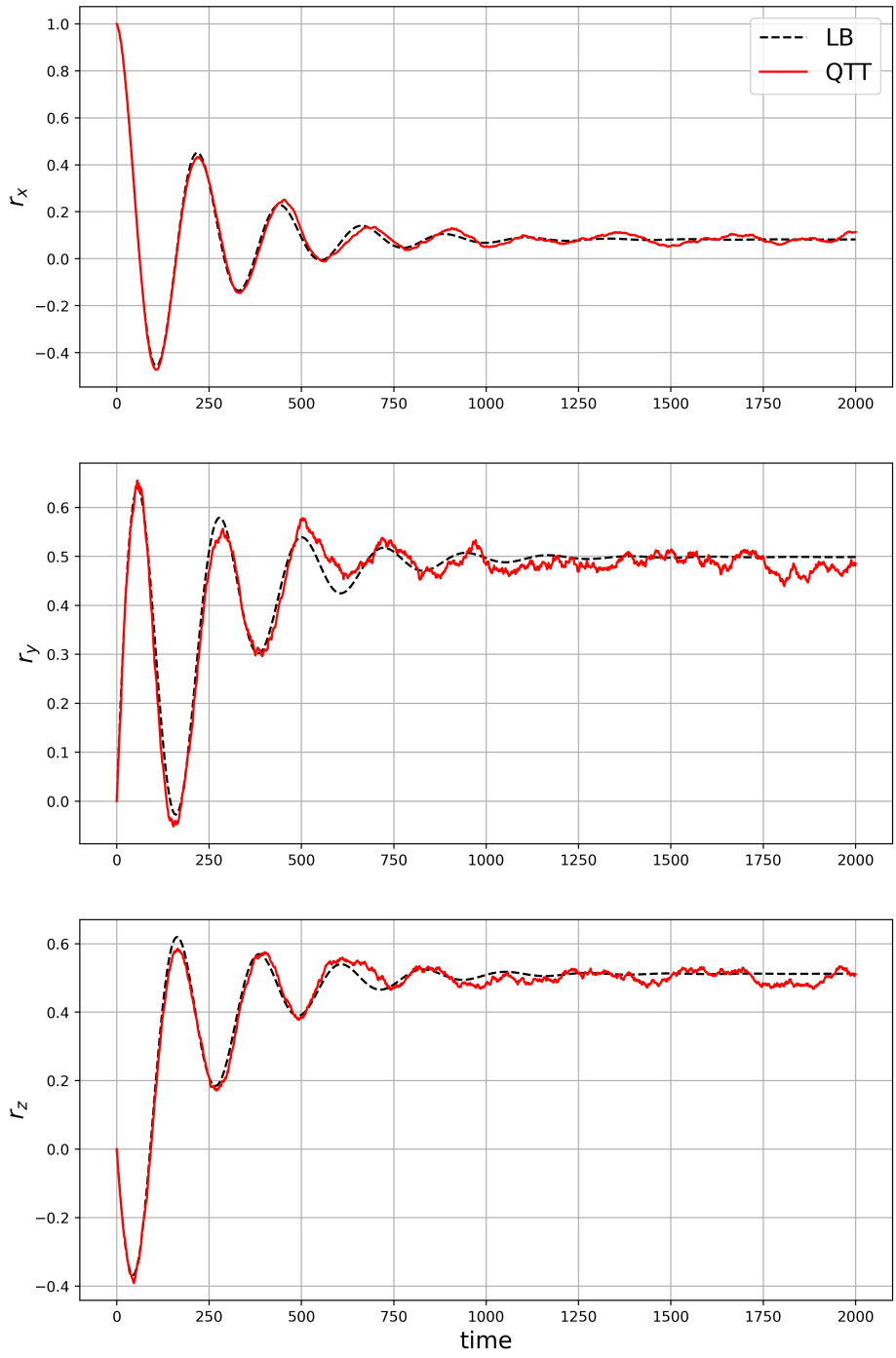

Figure 2.5: Trajectories simulation compared to the Lindblad master equation, with the system Hamiltonian as in equation (2.2) having $\Delta = 0.01$ and $\epsilon = 0.01$. Using the same simulation parameters as in figure 2.1, but with $S = 256$.

2.3.2 Measured frequency

Having successfully simulated quantum trajectories with an external signal Hamiltonian applied to the system, we now need to find the angular frequency of each trajectory. Synchronisation around the z-axis, with the angle ϕ about the z-axis. To do so, we find the angle ϕ from the x-axis in the xy-plane of the Bloch sphere, for each trajectory, using $\phi = \arctan(r_y/r_x)$, where r_x and r_y are the x and y components of the Bloch vector.

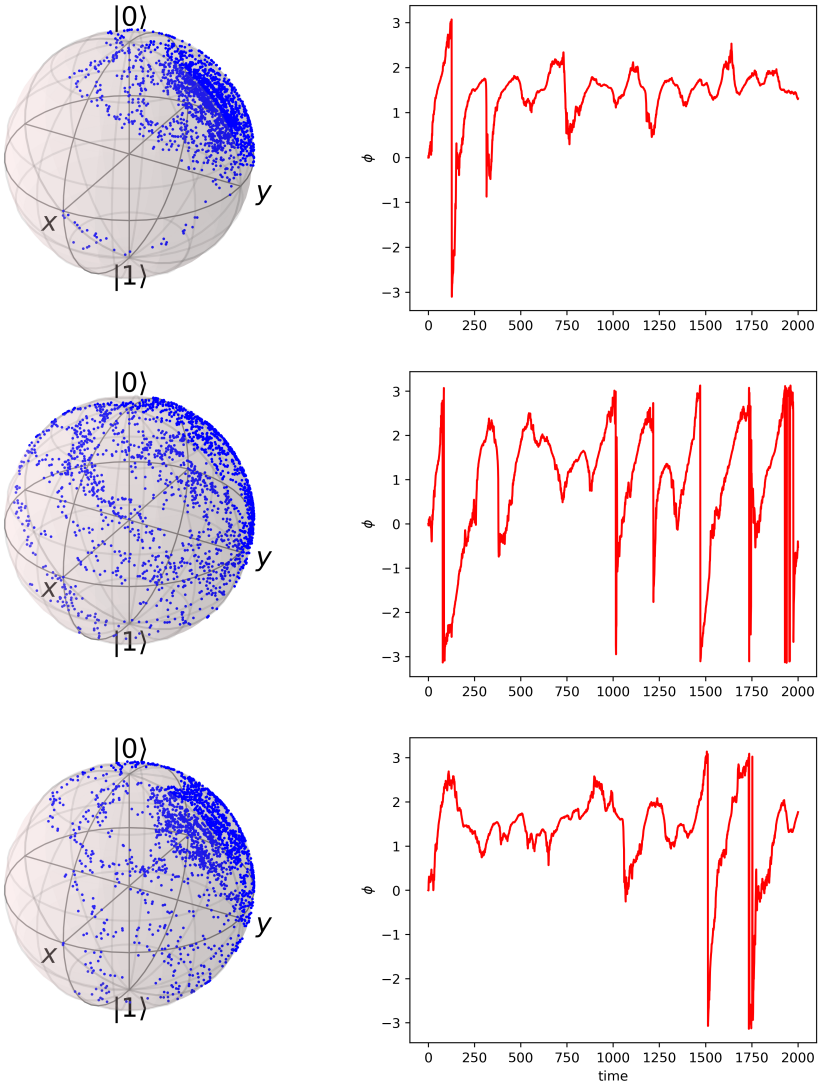

Figure 2.6: Single trajectories represented on the Bloch sphere in the left column, and the angle ϕ of the corresponding trajectories as a function of time in the right column. The parameters used for the trajectories are the same as in figure 2.5.

Next, we compute the accumulated angle Φ the trajectory has moved about the z-axis of the Bloch sphere. Having this we can compute a measured

angular frequency Ω for each trajectory from

$$\Omega = \frac{\Phi}{\tau},$$

where $\tau = N \times \delta t$ is the total simulation time. The accumulated angle Φ is found using the `numpy` function `unwrap`. This function detects each full rotation and let the angle accumulate indefinitely, thus, *unwrapping* the angle. With this we have the numerical tools necessary to simulate trajectories and measure the angular frequency of each. For a simulation of S trajectories we take the mean of the measured angular frequencies, and this is what is meant by Ω from here on out. Identifying frequency synchronisation can then be done by running quantum trajectory simulations where the detuning value Δ of the system Hamiltonian is changed, and for each value a measured angular frequency Ω is computed.

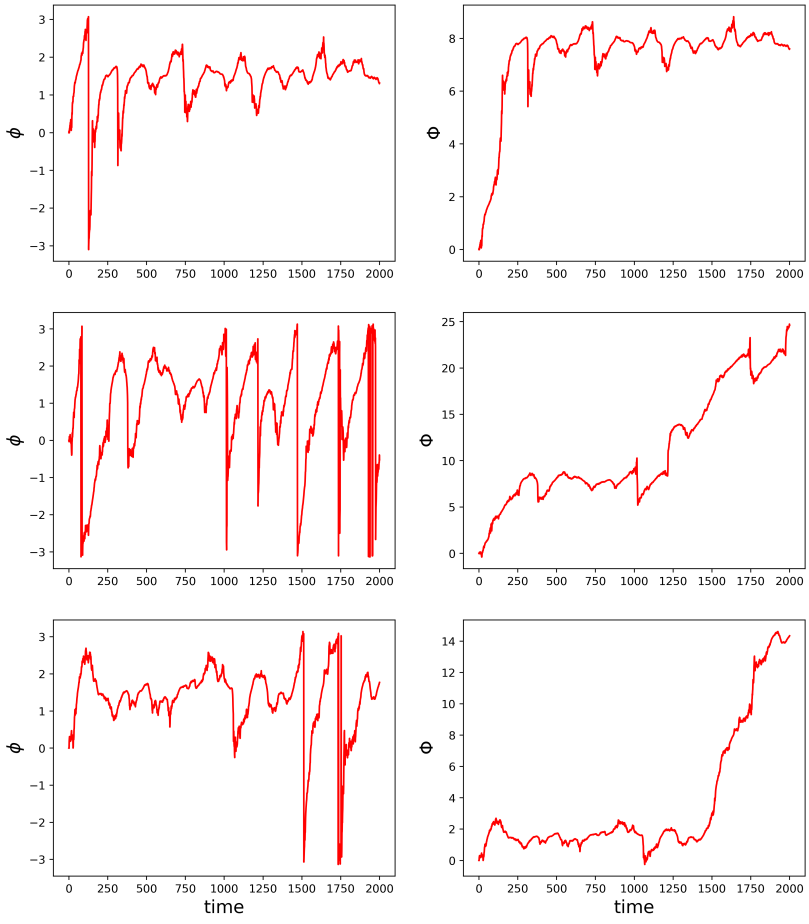

Figure 2.7: In this figure we show the angle ϕ as a function of time for the same trajectories as in figure 2.6 in the left column. The corresponding unwrapped angles are shown in the right column.

Chapter 3

Results

The results of the simulations indicate synchronisation behaviour similar to classical synchronisation with noise. We present the findings by plotting measured frequencies Ω against dentuning Δ. The standard deviation of the means, $\sigma_M = \sigma/\sqrt{S}$, is included for every second point as an error bar in the y-direction.

3.1 Frequency synchronisation

The main goal was to find a clear indication of frequency locking of a two-level system to an external signal. This was achieved using the model developed in the previous section, where the trajectories simulation was run for different detuning values, and the frequency of the resulting trajectories were measured. The average frequency Ω of each set of trajectories were then computed and plotted against the corresponding detuning value Δ. In figure 3.1 it was done for signal strength $\epsilon = 0.05, 0.01, 0.015$, and 0.02. The resulting plot clearly shows similar behaviour to the unbounded synchronisation region as shown in figure 1.5. A better view of the behaviour close for smaller Δ values is presented in 3.2, where we observe that the measured frequency only reaches zero when the detuning is zero.

To further illuminate effect of varying the singal strength, even smaller values of ϵ is presented in figure 3.3. Because the relative strength of the detuning has a larger span in this figure, we confirm that the measured frequency indeed approaches the natural frequency ω_0 of the system when the detuning is large compared to the signal strength. In all of the results, the synchronisation region increases with increased signal strength, which is exactly the behaviour we expect. This is consistent with the Arnold tongue 1.4 (c).

As per the observations made of the varying temperature in figure 2.4, when the temperature decreases, so does the observed noise in the system. We therefore replicated the signal strengths in figure 3.3, but for a temperature $T = 0.1$. The result is presented in figure 3.4. We observe that the synchronisation region increases when the temperature is decreased.

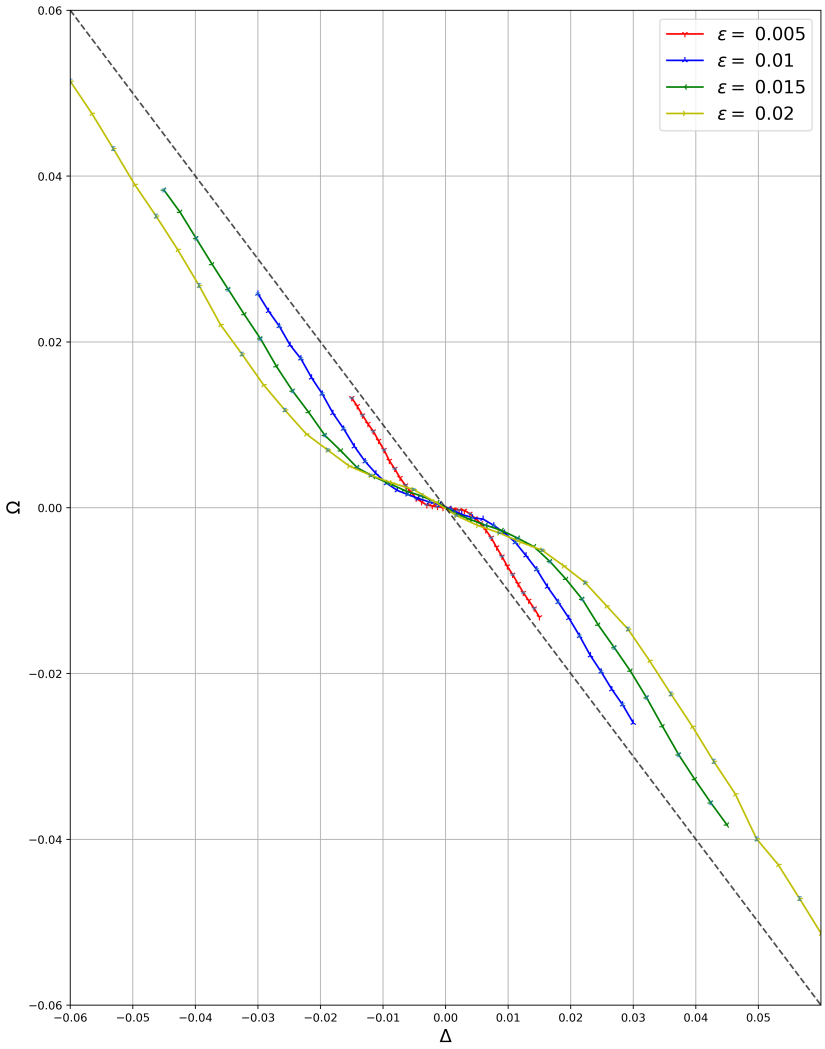

Figure 3.1: Measured angular frequency Ω plotted against detuning Δ. The trajectories simulations used to find the frequency data had $|E\rangle = |0\rangle$, measurements in the x-basis, $\theta = 0.01$, $\delta t = 0.01$, $T = 0.5$, $N = 4 \times 10^5$, $N_{\text{burnin}} = 1.5 \times 10^5$ and $S = 512$.

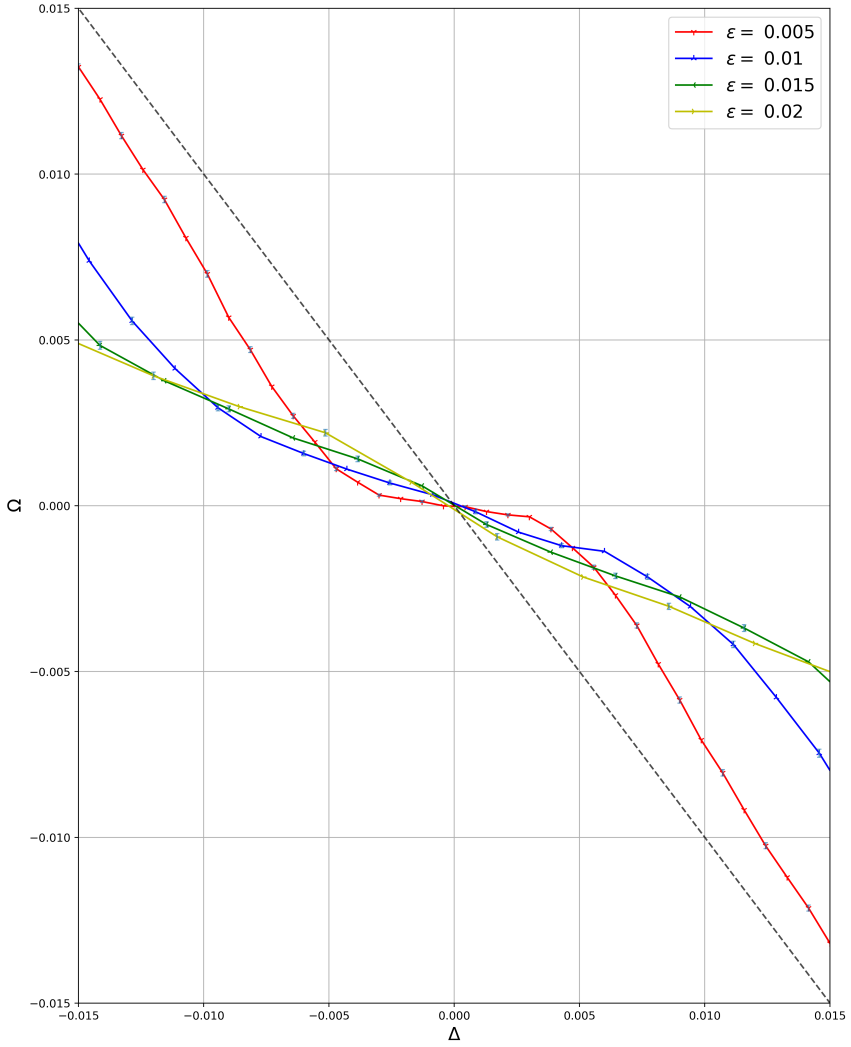

Figure 3.2: A closer look at the synchronisation region of figure 3.1.

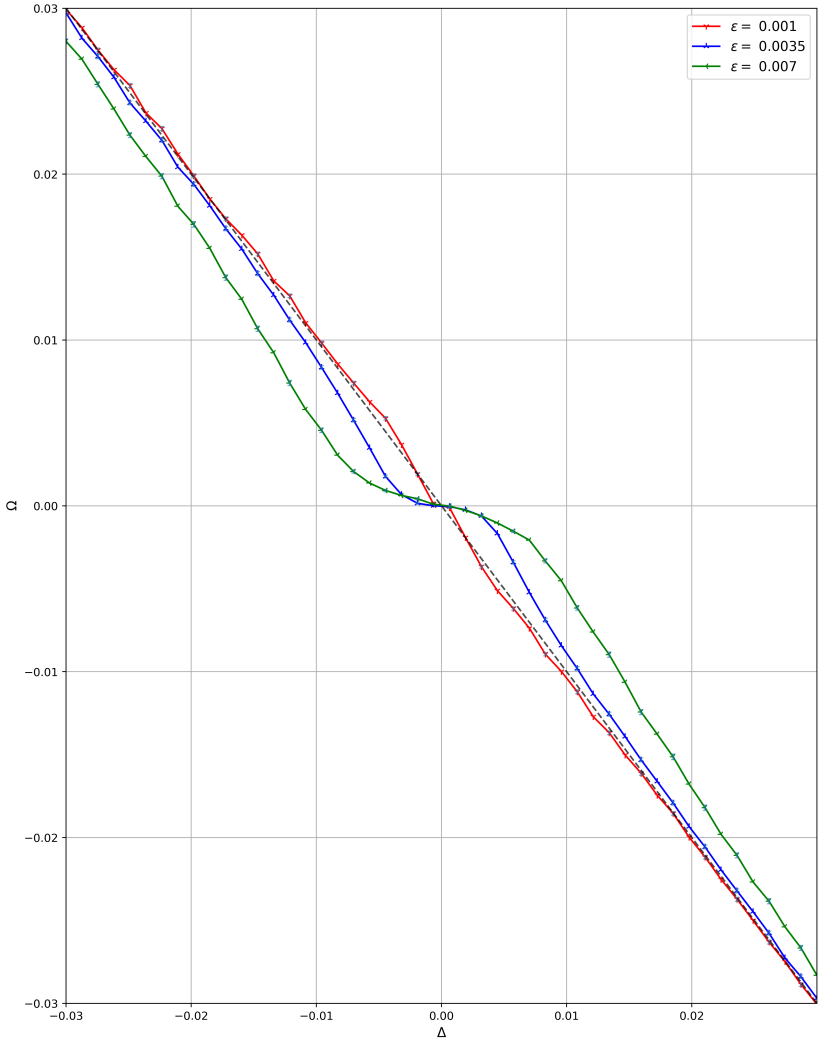

Figure 3.3: Measured angular frequency Ω plotted against detuning Δ, for smaller values of ϵ. Simulation parameters are the same as in figure 3.1, but with $S = 256$.

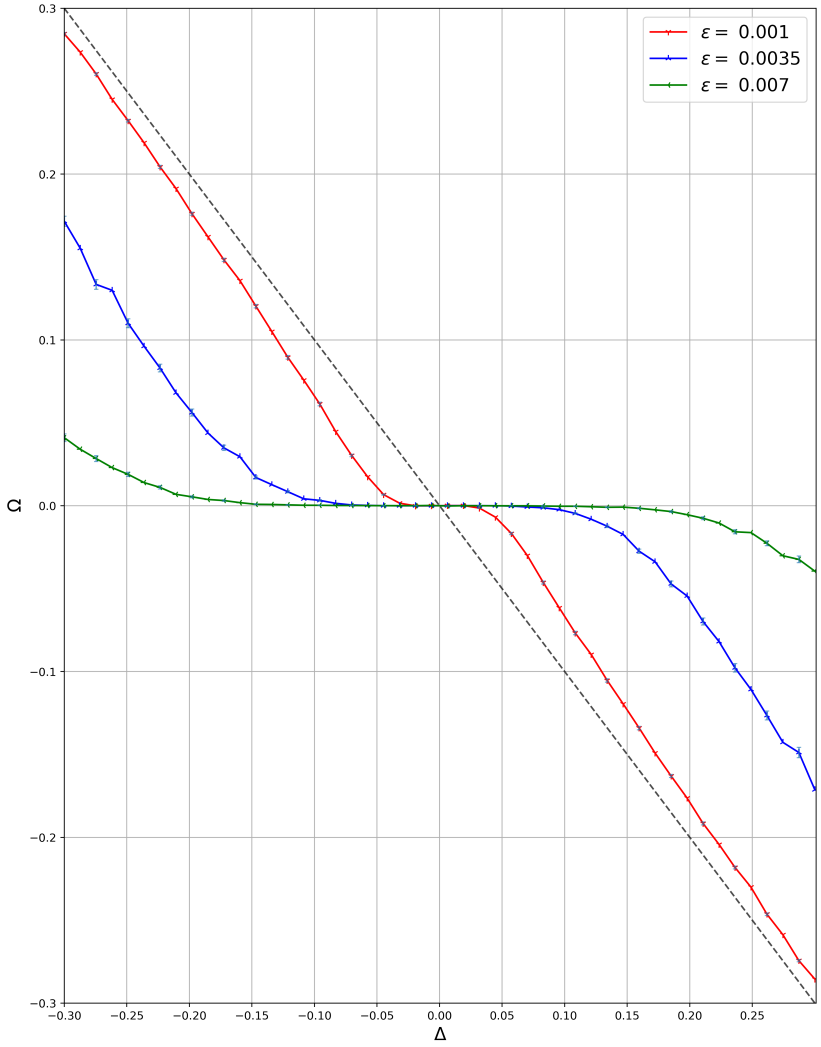

Figure 3.4: Same simulation parameters as in figure 3.3, but for temperature $T = 0.1$.

Chapter 4

Discussion and outlook

The results we obtained using our method clearly shows frequency synchronisation and subsequently does not require much discussion. However, we still wish to discuss the development of our method, the reasons for our choice of simulation parameters and possible improvements. Furthermore, the behaviour of trajectories resulting from different choice of environment and measurement basis is briefly discussed. Lastly, we give some ideas for setting up a model of two qubits using quantum trajectory theory.

4.1 Numerical method

The development of the numerical model was a long and tedious process of trial and error. We started by directly implementing the stochastic Schrödinger equations derived by Brun[4], successfully reproducing the Lindblad equation with one Lindblad operator. However, the Lindblad equation that we were looking for had to be found in some other way. After realising that two alternating interactions could be used, the implementation almost gave the expected results. The final piece of the puzzle was to correctly implement the measurements of the environment and the resulting updated system states. The main workhorse during this process has been to compare our results to the Lindblad equation.

Another hurdle came about when calculating the frequency of trajectories. Because of the randomness of the trajectories it proved hard to work out a general algorithm to keep track of their rotations on the Bloch sphere. An attempt at creating such an algorithm was made with some success. A variant using a fast Fourier transform was also made, but both methods failed to achieve very good results. In the end we luckily discovered, as so often is the case, that `numpy` had just the function we needed.

The choices made for simulation parameters, such as interaction strength θ, time step δt and temperature T, came about quite organically. After numerous tests it was clear that $\theta = \delta t = 0.01$ was a good choice since it gave relatively small errors and the simulations did not take too much time to accomplish. $T = 0.5$ was the standard choice when working on the implementation. As we have shown, lower temperatures have much less noise, and so using this value ensured that our implementation was working

as intended even with a fair amount of noise.

A good numerical improvement would be to estimate the burn-in time of the Monte Carlo method more rigorously. Our approach was to use the same initial state for every trajectory, often choosing $|\psi_0\rangle = |x_+\rangle$, and observe the time it took the system to reach the stationary state. This is not the correct way of estimating burn-in time. Instead, we should have chosen a random pure state, from the ensemble given by the stationary solution of the Lindblad equation. Analogous to the circle drawn on the Bloch sphere in figure 1.6. This way, the simulation would already be in the stationary state, and so the burn-in time could be properly estimated.

The presentation of the results could in principle always be improved upon. However, if not for the time constraint, a decent improvement would be represent the results in the Arnold tongue picture, as shown in figure 1.4. Additionally, we could scale the signal strength by the absorption rate Γ_+ to present our results in a similar fashion to other articles on synchronisation.

4.2 Interaction and measurement

The link between environment $|E\rangle$ and interactions $H_{\text{int}\pm}$ was explained in detail in section 2.1.1. For simplicity we have mostly used $|E\rangle = |0\rangle$ with the interaction it entails. Changing the choice of environment gives us a family of interactions on the form

$$H^z_{\text{int}\pm} = \frac{1}{4}(\sigma_x \otimes \sigma_x \pm \sigma_y \otimes \sigma_y),$$
$$H^x_{\text{int}\pm} = \frac{1}{4}(\sigma_x \otimes \sigma_y \pm \sigma_y \otimes \sigma_z),$$
$$H^y_{\text{int}\pm} = \frac{1}{4}(\sigma_x \otimes \sigma_x \mp \sigma_y \otimes \sigma_z).$$

Where we denote the choice of environment basis as z, x, y. Changing between the up and down states in the environment basis results in a sign change. As we saw in section 2.1.3, we may also measure the environment in any basis. The choice of environment and measurement basis were added to the numerical model, and results were compared to the Lindblad equation solution. The comparisons indicated a symmetry between interactions and measurement basis. We see this symmetry in figure 4.1, where the behaviour of the trajectories stay the same, but the measurement corresponding to the behaviours is permuted. This can also be seen by comparing figure 2.1 to 5.2, where we can see that the noise we get on the x and y Bloch vector component is swapped between the two methods.

Figure 4.1 compares single trajectories for environments in the z and x-basis, with measurements in z, x and y-basis, here we use the same random generator seed to highlight that the trajectory behaviour is completely equivalent. From this figure we also observe a likeness to the weak positive operator valued measurements explained in section 1.2.3. Having the environment in the same basis as the measurement seem to correspond to the first kind of weak measurement. This is represented as the green trajectory in 4.1 (a) and the blue trajectory in (b), we clearly observe the trajectories

"jumping" from one part of the sphere to another. For the measurements orthogonal to the environment we observe diffusive behaviour, corresponding to the second kind of weak measurement.

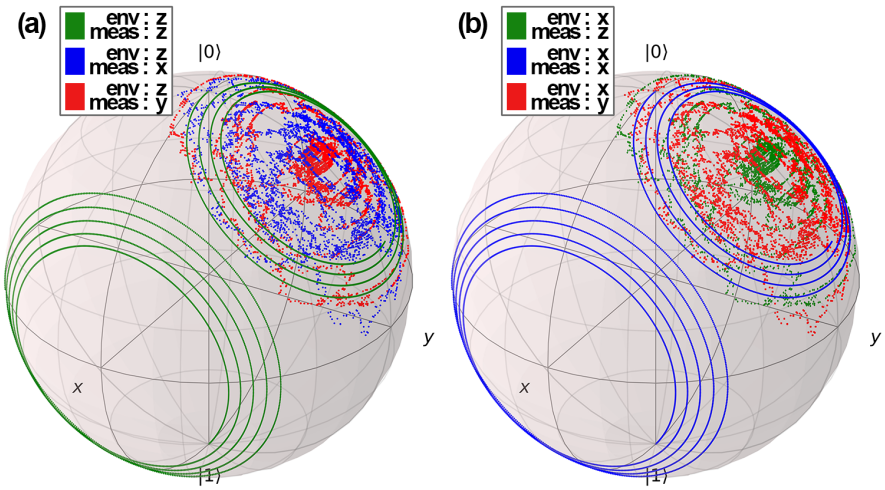

Figure 4.1: Comparing single trajectories with environment in the z-basis (a) and x-basis (b). Colours represent basis of measurement. The simulation parameters used were: $\theta = \delta t = 0.01$, $T = 0.1$, $\epsilon = 0.001$ and $\Delta = 0.05$.

4.3 Two-qubit synchronisation

Investigating synchronisation between two qubits would be interesting, but also mean that a big part of our model must be reworked. Here we express some initial thoughts about how this could be achieved. We can use the Heisenberg interaction for the coupling between the two qubits, which can be written on the form

$$\sigma_-^1\sigma_+^2 + \sigma_+^1\sigma_-^2 = \frac{1}{2}(\sigma_x^1\sigma_x^2 + \sigma_y^1\sigma_y^2),$$

where the superscript 1 and 2 refers to qubit 1 and 2. Both qubits will also evolve with their respective Hamiltonians $H_{\text{sys}} = \omega_0\sigma_z/2$. Figure 4.2 shows what this system could look like using the trajectory method. Before any of the qubits interact with the environment, they interact with each other, leaving us with an entangled state. Suppose we then interact each qubit with an environment state. Assuming the environment states only interact with their respective qubits, it should be possible to obtain a pure state for the qubits after measurement. This can likely be thought of as first interacting and measuring one environment state, before doing the same for the environment state interacting with the other qubit. We then let each system evolve one time step with their respective system Hamiltonian. The process is then repeated. The method as described is clearly very simplified, but could provide a starting point for further investigation.

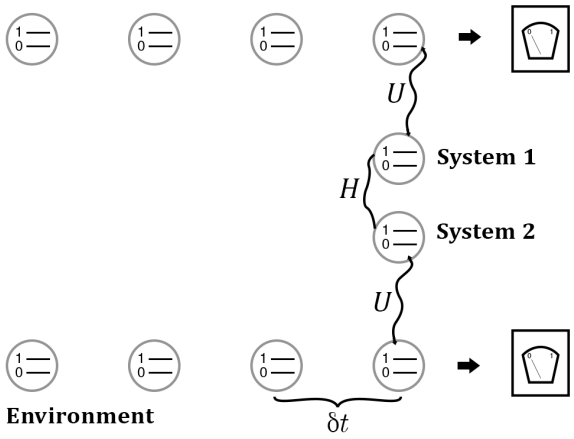

Figure 4.2: A schematic outlining the general idea of a two qubit trajectory model. System 1 and 2 have some interaction Hamiltonian H, and the environment states successively pass by interacting with each of the systems before being measured.

Chapter 5

Appendix

Here, the excess derivations, longer and unnecessary calculations, extra figures and so forth are presented. As is the nature of the appendix.

5.1 Derivation of evolved system density matrix expansion

Deriving the expansion to the second order in θ for the evolved system density matrix ρ'_S.

We have the unitary operator

$$U = \exp\left\{-i\theta \sum_j A_j \otimes B_j\right\},$$

where A_j and B_j are hermitian operators acting on the Hilbert space of the system and environment respectively. Additionally, we have $\theta \ll 1$. First we expand U to second order in θ

$$U \approx \mathbb{1} - i\theta A_j \otimes B_j - \frac{\theta^2}{2} A_j A_{j'} \otimes B_j B_{j'},$$

where we simplify the notation slightly by not explicitly writing the summation. We then insert this approximation into our expression for the

evolved system density matrix and find all terms up to second order in θ.

$$\begin{aligned}
\rho'_S &= \mathrm{Tr}_E\left[U\left|\psi\right\rangle\left\langle\psi\right|\otimes\left|E\right\rangle\left\langle E\right|U^\dagger\right] \\
&\approx \mathrm{Tr}_E\left[\left(\mathbb{1}-i\theta A_j\otimes B_j-\frac{\theta^2}{2}A_jA_{j'}\otimes B_jB_{j'}\right)\left|\psi\right\rangle\left\langle\psi\right|\right. \\
&\quad\left.\otimes\left|E\right\rangle\left\langle E\right|\left(\mathbb{1}+i\theta A_j^\dagger\otimes B_j^\dagger-\frac{\theta^2}{2}A_j^\dagger A_{j'}^\dagger\otimes B_j^\dagger B_{j'}^\dagger\right)\right] \\
&= \left|\psi\right\rangle\left\langle\psi\right|-i\theta A_j\left|\psi\right\rangle\left\langle\psi\right|\mathrm{Tr}_E\left[B_j\left|E\right\rangle\left\langle E\right|\right] \\
&\quad+i\theta\left|\psi\right\rangle\left\langle\psi\right|A_j^\dagger\,\mathrm{Tr}_E\left[\left|E\right\rangle\left\langle E\right|B_j^\dagger\right] \\
&\quad+\theta^2A_j\left|\psi\right\rangle\left\langle\psi\right|A_{j'}^\dagger,\mathrm{Tr}_E\left[B_j\left|E\right\rangle\left\langle E\right|B_{j'}^\dagger\right] \\
&\quad-\frac{\theta^2}{2}A_jA_{j'}\left|\psi\right\rangle\left\langle\psi\right|\mathrm{Tr}_E\left[B_jB_{j'}\left|E\right\rangle\left\langle E\right|\right] \\
&\quad-\frac{\theta^2}{2}\left|\psi\right\rangle\left\langle\psi\right|A_j^\dagger A_{j'}^\dagger,\mathrm{Tr}_E\left[\left|E\right\rangle\left\langle E\right|B_j^\dagger B_{j'}^\dagger\right]
\end{aligned}$$

Working out the traces over the environment we find

$$\begin{aligned}
\mathrm{Tr}_E\left[B_j\left|E\right\rangle\left\langle E\right|\right] &= \sum_{E'}\left\langle E'\right|B_j\left|E\right\rangle\left\langle E\middle|E'\right\rangle = \sum_{E'}\left\langle E\middle|E'\right\rangle\left\langle E'\right|B_j\left|E\right\rangle \\
&= \left\langle E\right|\sum_{E'}\left|E'\right\rangle\left\langle E'\right|B_j\left|E\right\rangle = \left\langle E\right|B_j\left|E\right\rangle \\
\mathrm{Tr}_E\left[\left|E\right\rangle\left\langle E\right|B_j^\dagger\right] &= \sum_{E'}\left\langle E'\middle|E\right\rangle\left\langle E\right|B_j\left|E'\right\rangle \\
&= \left\langle E\right|B_j\sum_{E'}\left|E'\right\rangle\left\langle E'\middle|E\right\rangle = \left\langle E\right|B_j\left|E\right\rangle, \quad B_j = B_j^\dagger \\
\mathrm{Tr}_E\left[B_j\left|E\right\rangle\left\langle E\right|B_{j'}^\dagger\right] &= \sum_{E'}\left\langle E'\right|B_j\left|E\right\rangle\left\langle E\right|B_{j'}\left|E'\right\rangle \\
&= \left\langle E\right|B_{j'}\sum_{E'}\left|E'\right\rangle\left\langle E'\right|B_j\left|E\right\rangle = \left\langle E\right|B_{j'}B_j\left|E\right\rangle \\
\mathrm{Tr}_E\left[B_jB_{j'}\left|E\right\rangle\left\langle E\right|\right] &= \sum_{E'}\left\langle E'\right|B_jB_{j'}\left|E\right\rangle\left\langle E\middle|E'\right\rangle \\
&= \left\langle E\right|\sum_{E'}\left|E'\right\rangle\left\langle E'\right|B_jB_{j'}\left|E\right\rangle = \left\langle E\right|B_jB_{j'}\left|E\right\rangle.
\end{aligned}$$

As with the first trace, the last one is identical to its hermitian conjugate. Inserting these into our previous equation, we get

$$\begin{aligned}
\rho'_S &\approx \left|\psi\right\rangle\left\langle\psi\right|-i\theta(A_j\left|\psi\right\rangle\left\langle\psi\right|\left\langle E\right|B_j\left|E\right\rangle-\left|\psi\right\rangle\left\langle\psi\right|A_j\left\langle E\right|B_j\left|E\right\rangle) \\
&\quad+\frac{\theta^2}{2}\Big(2A_j\left|\psi\right\rangle\left\langle\psi\right|A_{j'}\left\langle E\right|B_{j'}B_j\left|E\right\rangle \\
&\quad-A_jA_{j'}\left|\psi\right\rangle\left\langle\psi\right|\left\langle E\right|B_{j'}B_j\left|E\right\rangle-\left|\psi\right\rangle\left\langle\psi\right|A_jA_{j'}\left\langle E\right|B_{j'}B_j\left|E\right\rangle\Big) \\
&= \left|\psi\right\rangle\left\langle\psi\right|-i\theta[A_j,\left|\psi\right\rangle\left\langle\psi\right|]\left\langle E\right|B_j\left|E\right\rangle+\frac{\theta^2}{2}\left\langle E\right|B_{j'}B_j\left|E\right\rangle \\
&\quad\times\Big(2A_j\left|\psi\right\rangle\left\langle\psi\right|A_{j'}-A_jA_{j'}\left|\psi\right\rangle\left\langle\psi\right|-\left|\psi\right\rangle\left\langle\psi\right|A_jA_{j'}\Big)
\end{aligned}$$

5.2 Figures

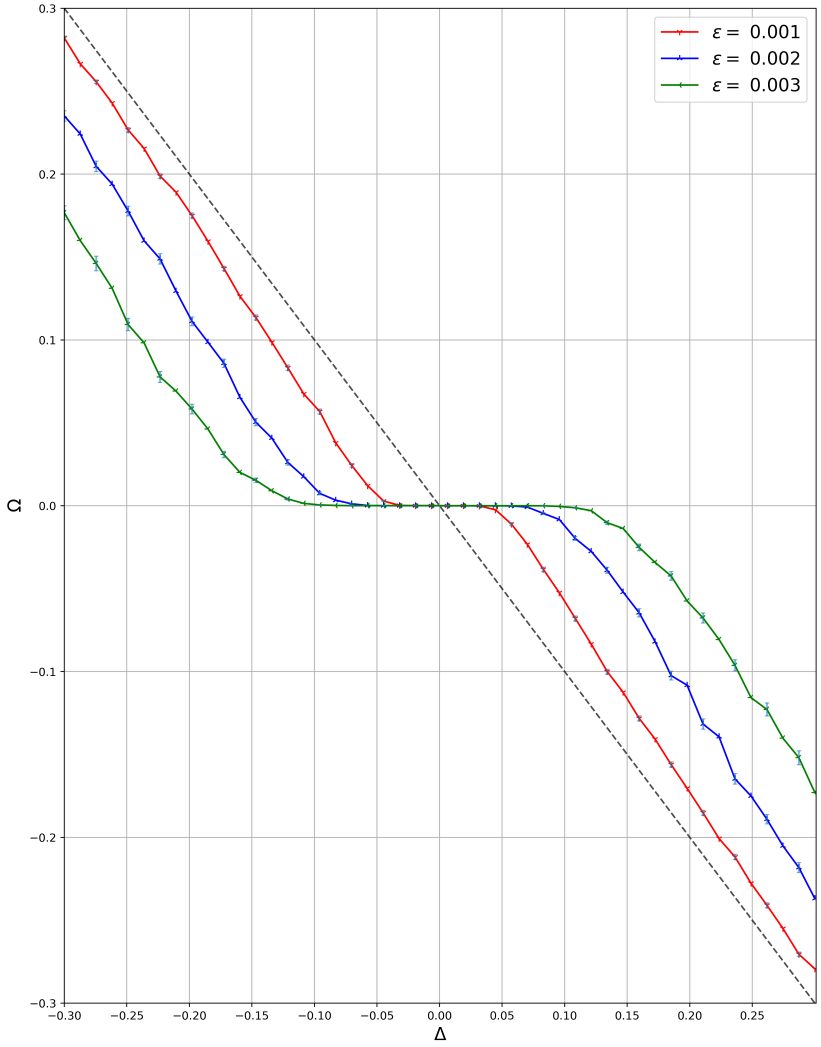

Figure 5.1: Measured frequency against detuning, using $|E\rangle = |y_-\rangle$ with measurements taken in the z-basis. Parameters same as in figure 3.4.

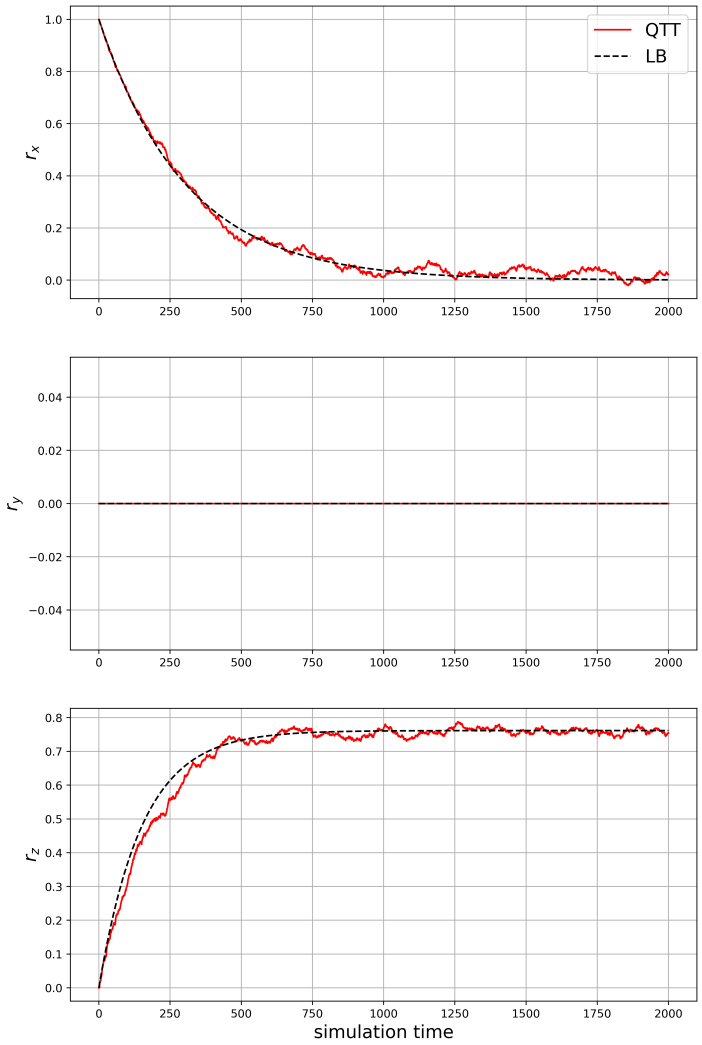

Figure 5.2: Trajectory method compared to the Lindblad solution. Simulation using $|E\rangle = |y_-\rangle$ and measurements taken in the z-basis. Parameters same as in figure 2.1, with $S = 256$.

Bibliography

[1] Alexandre Roulet and Christoph Bruder. 'Synchronizing the Smallest Possible System'. In: *Physical review letters* 121.5 (2018), pp. 053601–053601. ISSN: 0031-9007.

[2] Álvaro Parra-López and Joakim Bergli. 'Synchronization in two-level quantum systems'. In: *Physical review. A* 101.6 (2020). ISSN: 2469-9926.

[3] Liyun Zhang et al. *Observing Quantum Synchronization of a Single Trapped-Ion Qubit*. 2022. DOI: 10.48550/ARXIV.2205.05936. URL: https://arxiv.org/abs/2205.05936.

[4] Todd A Brun. 'A simple model of quantum trajectories'. In: *American journal of physics* 70.7 (2002), pp. 719–737. ISSN: 0002-9505.

[5] Seung-Bo Shim, Matthias Imboden and Pritiraj Mohanty. 'Synchronized Oscillation in Coupled Nanomechanical Oscillators'. In: *Science (American Association for the Advancement of Science)* 316.5821 (2007), pp. 95–99. ISSN: 0036-8075.

[6] Arkady Pikovsky, Michael Rosenblum and Jürgen Kurths. *Synchronization: A Universal Concept in Nonlinear Sciences*. Cambridge: Cambridge University Press, 2001. ISBN: 052153352X.

[7] Balth. van der Pol Jun. D.Sc. 'LXXXVIII. On "relaxation-oscillations"'. In: *The London, Edinburgh, and Dublin Philosophical Magazine and Journal of Science* 2.11 (1926), pp. 978–992. DOI: 10.1080/14786442608564127. eprint: https://doi.org/10.1080/14786442608564127. URL: https://doi.org/10.1080/14786442608564127.

[8] Tony E. Lee and H.R. Sadeghpour. 'Quantum synchronization of quantum van der Pol oscillators with trapped Ions'. In: *Physical review letters* 111.23 (2013), pp. 234101–234101. ISSN: 0031-9007.

[9] Stefan Walter, Andreas Nunnenkamp and Christoph Bruder. 'Quantum synchronization of two Van der Pol oscillators'. In: *ANNALEN DER PHYSIK* 527.1-2 (2015), pp. 131–138. ISSN: 0003-3804.

[10] C.A. Holmes, C.P. Meaney and G.J. Milburn. 'Synchronization of many nanomechanical resonators coupled via a common cavity field'. In: *Physical review. E, Statistical, nonlinear, and soft matter physics* 85.6 (2012), pp. 066203–066203. ISSN: 1539-3755.

[11] Arif Warsi Laskar et al. 'Observation of Quantum Phase Synchronization in Spin-1 Atoms'. In: *Physical review letters* 125.1 (2020), pp. 1–013601. ISSN: 0031-9007.

[12] Roson Nongthombam, Sampreet Kalita and Amarendra K. Sarma. *Synchronization of a superconducting qubit to an optical field mediated by a mechanical resonator*. 2022. DOI: 10.48550/ARXIV.2205.12214. URL: https://arxiv.org/abs/2205.12214.

[13] Benedetto Militello and Anna Napoli. 'Synchronizing Two Superconducting Qubits through a Dissipating Resonator'. In: *Entropy (Basel, Switzerland)* 23.8 (2021), p. 998. ISSN: 1099-4300.

[14] H. Carmichael and U. de Bruxelles. *An Open Systems Approach to Quantum Optics: Lectures Presented at the Université Libre de Bruxelles, October 28 to November 4, 1991*. An Open Systems Approach to Quantum Optics: Lectures Presented at the Université Libre de Bruxelles, October 28 to November 4, 1991 v. 18. Springer Berlin Heidelberg, 1993. ISBN: 9783540566342. URL: https://books.google.no/books?id=El5gxgxWhpgC.

[15] Daniel Manzano. 'A short introduction to the Lindblad Master Equation'. In: (2019).

[16] J.R. Johansson, P.D. Nation and Franco Nori. 'QuTiP 2: A Python framework for the dynamics of open quantum systems'. In: *Computer Physics Communications* 184.4 (2013), pp. 1234–1240. ISSN: 0010-4655. DOI: https://doi.org/10.1016/j.cpc.2012.11.019. URL: https://www.sciencedirect.com/science/article/pii/S0010465512003955.